NASA TECHNICAL NOTE

NASA TN D-4206

NASA TN D-4206

RADIO-FREQUENCY INDUCTION HEATING OF LOW-PRESSURE PLASMAS

by Ronald J. Sovie and George R. Seikel

Lewis Research Center
Cleveland, Ohio

NATIONAL AERONAUTICS AND SPACE ADMINISTRATION • WASHINGTON, D. C. • OCTOBER 1967

NASA TN D-4206

RADIO-FREQUENCY INDUCTION HEATING OF LOW-PRESSURE PLASMAS

By Ronald J. Sovie and George R. Seikel

Lewis Research Center
Cleveland, Ohio

NATIONAL AERONAUTICS AND SPACE ADMINISTRATION

For sale by the Clearinghouse for Federal Scientific and Technical Information
Springfield, Virginia 22151 – CFSTI price $3.00

RADIO-FREQUENCY INDUCTION HEATING OF LOW-PRESSURE PLASMAS*

by Ronald J. Sovie and George R. Seikel

Lewis Research Center

SUMMARY

Induction heating of a low-density cylindrical plasma is investigated experimentally and analytically; in particular, the ohmic power dissipation and energy storage in the plasma are studied. The experimental values for both quantities are in good agreement with the theoretical results.

The theoretical treatment consists of a linearized analysis of the coupling of a solenoidal radio-frequency magnetic field and a steady cylindrical plasma. The plasma is assumed to have uniform electron density, electron temperature, and resistivity. An important feature of this analysis is that the inertia term is retained in the Ohm's law of the plasma. The ratio of this term to the resistive term is of order $\omega\tau$ (the product of the applied frequency and the electron collision time). The effect of the inertia term is to permit deeper penetration of the applied field into the plasma. The power dissipated and average energy stored in the plasma over a cycle are calculated by evaluating the complex Poynting vector at the plasma surface. The effect of the energy storage is to reduce the inductance of the radio-frequency coil. An interesting result of this analysis is that for low pressure plasmas this inductance change is a function of electron density only. This result indicates that a plasma may possibly be generated and diagnosed with the same radio-frequency coil.

The experiments were conducted in helium at pressures of 3 to 20 microns with a 17.5-megahertz, 2-kilowatt radio-frequency power supply. The discharge tube was 4.8 centimeters in diameter. The power was coupled to the plasma by a 4 turn 7.7-centimeter-long, 7.5-centimeter-diameter Faraday shielded radio-frequency coil. The power dissipated, the average energy stored in the plasma, and the radio-frequency magnetic field were determined from detailed electrical circuit measurements. To compare theory and experiment, line ratio spectroscopy and microwave interferometry were used to determine the electron temperature and density, respectively. Power transfer efficiencies as high as 73 percent were obtained with 650 watts being coupled to the plasma.

---

*Preliminary results of this investigation were presented at the 8th annual APS Plasma Physics meeting, Nov. 2 to 5, 1966, Boston, Mass.

INTRODUCTION

The excitation of gases by means of an electrodeless induction discharge has a long history dating from the early work of Hittorf (ref. 1) who first observed that an electrical discharge could be produced in a gas tube by induction from a coil surrounding the tube. The radio-frequency (r-f) electrodeless discharge has been useful through the years as a spectroscopic light source (ref. 2). In recent years, interest has been renewed in the r-f induction heating discharge as a plasma or ion source for plasma propulsion devices and in connection with energy addition to flowing gases (ref. 3). The use of r-f induction heating as a plasma source is advantageous in that acceptable power transfer efficiencies are attainable while the problem of electrode erosion is eliminated. An analysis of the coupling between a solenoidal r-f magnetic field and a steady cylindrical plasma may also aid in understanding the basic mechanisms in low-pressure plasma acceleration devices such as the travelling magnetic-wave accelerator (ref. 4).

The present theoretical and experimental analysis of r-f induction heating was conducted to determine the basic plasma properties and power transfer efficiencies as functions of the external circuit parameters. The theory is developed and solutions are obtained for the power coupled to the plasma and the inductance change of the r-f coil. The experimental arrangement and diagnostics needed to compare experiment with theory are then described. Finally, the experimental and theoretical results are compared and discussed.

THEORY

Assumptions and General Equations

In this treatment, the plasma and r-f coil are considered to be coaxial circular cylinders of sufficient length that end effects may be neglected. The coupling is considered to be purely inductive and, therefore, there are no axial electric fields or currents. Furthermore, it is assumed that only alternating currents appear with no charge buildup. For tube radii in the centimeter range and megacycle field frequencies, displacement currents are negligible and Maxwell's equations take the form

$$\nabla \cdot \vec{D} = 0 \tag{1}$$

$$\nabla \cdot \vec{B} = 0 \tag{2}$$

$$\nabla \times \vec{E} = -\frac{\partial \vec{B}}{\partial t} \tag{3}$$

$$\nabla \times \vec{H} = \vec{j} \tag{4}$$

where $\vec{B} = \mu_0 \vec{H}$ and $\vec{D} = \epsilon_0 \vec{E}$. (Rationalized SI units are used throughout this report, and all symbols are defined in appendix A.) The dielectric constant ϵ_0 and magnetic permeability μ_0 are assumed to be the same in the plasma as in free space.

The linearized Ohm's law for the plasma, including electron inertia, is

$$\frac{m_e}{n_e q^2} \frac{\partial \vec{j}}{\partial t} = \vec{E} - \eta \vec{j} \tag{5}$$

where the electron density, n_e and resistivity $\eta = \dfrac{m_e \nu_c}{n_e q^2}$ are assumed to be uniform throughout the plasma. In actuality, the electron density and resistivity are not uniform along the plasma radius. However, the assumption made is that these spatially dependent quantities may be replaced by a uniform electron density and resistivity which represents the effective values of these quantities (Eckert, ref. 5).

In the subsequent analysis, only the azimuthal component of equation (5) is used. The previous assumptions of no charge buildup and $\vec{j}_z = 0$ require that $\vec{j}_r = 0$. Thus, no loss in generality results from ignoring either the $\vec{j} \times \vec{B}$ or ∇_p terms in the generalized Ohm's law (ref. 6), since these terms are identically zero in the azimuthal direction. The only other term in the generalized Ohm's law (ref. 6) that may not be of higher order and is neglected in equation (5) is the $\vec{v} \times \vec{B}$ term. This term will be present only in the presence of a direct-current magnetic field. However, for sufficiently small direct-current magnetic fields this term may be neglected.

Formation of Complex Poynting Vector

The complex Poynting vector will now be formed in order to obtain solutions for the power dissipated in the plasma and the energy stored in the plasma. Since equations (1) to (5) are linear, the following separation of variables is made

$$\vec{E}(r, t) = \vec{E}(r) e^{i\omega t} \tag{6a}$$

$$\vec{B}(r, t) = \vec{B}(r) e^{i\omega t} \tag{6b}$$

$$\vec{j}(r, t) = \vec{j}(r) e^{i\omega t} \tag{6c}$$

Using equations (6a) to 6(c) reduces equations (3), (4), and (5) to

$$\nabla \times \vec{E}(r) = -i\omega\vec{B}(r) \tag{7}$$

$$\nabla \times \vec{B}(r) = \mu_0 \vec{j}(r) \tag{8}$$

$$\left(\eta + i\frac{m_e\omega}{n_e q^2}\right)\vec{j}(r) = \vec{E}(r) \tag{9}$$

where $\vec{E}(r)$, $\vec{B}(r)$, and $\vec{j}(r)$ are complex time independent vectors whose amplitudes correspond to the physical peak values. In most of the subsequent equations only their dependence on r will be understood.

The complex conjugate of equation (8) is

$$\nabla \times \vec{B}^* = \mu_0 \vec{j}^* \tag{10}$$

Forming the scalar product of equation (10) with $\vec{E}$ and equation (7) with $-\vec{B}^*$ and adding yields

$$\vec{E} \cdot \left(\nabla \times \vec{B}^*\right) - \vec{B}^* \cdot \left(\nabla \times \vec{E}\right) = \mu_0 \vec{j}^* \cdot \vec{E} + i\omega\vec{B} \cdot \vec{B}^*$$

which becomes, on regrouping terms and using equation (9),

$$-\frac{1}{\mu_0} \nabla \cdot \left(\frac{1}{2} \vec{E} \times \vec{B}^*\right) = \frac{1}{2} \vec{j} \cdot \vec{j}^* \left(\eta + i\frac{m_e\omega}{n_e q^2}\right) + 2i\omega\left(\frac{\frac{1}{2}\vec{B} \cdot \vec{B}^*}{2\mu_0}\right) \tag{11}$$

Equation (11) is an extension of the result given by Abraham and Becker (ref. 7, p. 202, eq. (9)).[1] After integrating equation (11) over the volume and using the divergence theorem, the result can be written

$$-\frac{1}{\mu_0} \int_S \frac{1}{2} \left(\vec{E} \times \vec{B}^*\right) \cdot d\vec{S} = \overline{W} + 2i\omega\overline{U} \tag{12a}$$

where

[1]The authors are indebted to Dr. F. A. Lyman for noting this similarity and pointing out that it could be generalized to include the case considered herein.

$$\overline{W} = \int_V \eta\left(\frac{1}{2}\,\vec{j}\cdot\vec{j}^{\,*}\right)dV = \int_V \eta\,\overline{\left[\mathrm{Re}(\vec{j})\right]^2}\,dV \tag{12b}$$

$$\overline{U} = \overline{U}_M + \overline{U}_{ke} \tag{12c}$$

$$\overline{U}_M = \int_V \frac{1}{2\mu_0}\left(\frac{1}{2}\,\vec{B}\cdot\vec{B}^{\,*}\right)dV = \int_V \frac{1}{2\mu_0}\,\overline{\left[\mathrm{Re}(\vec{B})\right]^2}\,dV \tag{12d}$$

$$U_{ke} = \int_V \frac{1}{2}\,\frac{m_e}{n_e q^2}\left(\frac{1}{2}\,\vec{j}\cdot\vec{j}^{\,*}\right)dV = \int_V \frac{1}{2}\,\frac{m_e}{n_e q^2}\,\overline{\left[\mathrm{Re}(\vec{j})\right]^2}\,dV \tag{12e}$$

The physical meanings of the various terms in equations (12) are as follows. Since $\overline{\left[\mathrm{Re}(\vec{j})\right]^2}$ is the time average of the square of the real current density over a cycle, the quantity $\overline{W}$ represents the average rate of joule dissipation; that is, the average power expended during a cycle in resistive heating of the plasma. By similar reasoning, $\overline{U}_M$ is seen to be the average energy stored in the magnetic field during a cycle. The foregoing two terms are those expected for an ordinary solid conductor in a time-varying magnetic field. The term $\overline{U}_{ke}$, however, is not so intuitively obvious; in fact, it usually is not considered in analyses of the r-f heating of solid conductors. It arises in the present analysis because of the importance of electron inertia in low-pressure r-f plasmas. By writing the real current density as $\mathrm{Re}(\vec{j}) = n_e q \vec{v}_e$, this term becomes

$$\overline{U}_{ke} = \int_V n_e\,\frac{1}{2}\,m_e\overline{v_e^2}\,dV$$

which clearly shows that $\overline{U}_{ke}$ is the time average of the kinetic energy invested in the drift motion of the plasma electrons.[2] Both $\overline{U}_{ke}$ and $\overline{U}_M$ contribute to the plasma

[2]It is possible to prove in general, that, for a fully ionized plasma with no mean velocity, $\overline{U}_{ke}$ is the sum of the time-averaged electron and ion drift kinetic energy. But in the present case, it can be demonstrated that the azimuthal ion drift velocity is m_e/m_i times the electron drift velocity, since the plasma as a whole has no motion in the azimuthal direction (note that $(\vec{j}\times\vec{B})_\theta = 0$ because $\vec{j}_r = \vec{j}_z = 0$). Hence, the ion drift kinetic energy is negligible compared with that of the electrons.

reactance, as is clear from equation (12a).

Equation (12a) will be used in the following manner. The complex Poynting vector $(\vec{E} \times \vec{B}^*)/\mu_0$ will be evaluated at the surface of the plasma, so that the quantity on the left hand side of equation (12a) is known. Taking the real part of this quantity will then yield the average resistive power $\overline{W}$. The average energy stored in the plasma during a cycle $\overline{U}$ will be obtained from the imaginary part of $-\int_S \left(\vec{E} \times \vec{B}^*/2\mu_0\right) \cdot dS$. An effective inductance of the plasma L_p can then be defined by the relation

$$\frac{1}{2} L_p \overline{I^2} = \overline{U} \tag{13}$$

where $\overline{I^2}$ is the mean-square current in the r-f coil.

Solution for Magnetic and Electric Fields

In order to evaluate the quantity on the left side of equation (12a), it is necessary to solve equations (7), (8), and (9) for $\vec{B}$ and $\vec{E}$. It is convenient to introduce two parameters that will be used throughout this report, namely

$$\alpha = \frac{m_e \omega}{\eta n_e q^2} = \frac{\omega}{\nu_c} = \omega\tau \tag{14}$$

and

$$\delta = \left(\frac{2\eta}{\mu_0 \omega}\right)^{1/2} \tag{15}$$

where α is the ratio of the r-f field frequency to the collision frequency ν_c and δ is the normal r-f skin depth.

The following equation for $\vec{B}$ is obtained by substituting equations (9) and (14) into equation (8) and taking the curl of both sides

$$\nabla \times \nabla \times \vec{B} = -\frac{i\mu_0 \omega}{\eta(1 + i\alpha)} \vec{B} \tag{16}$$

Noting that $\vec{B} = B\vec{z}$ and rearranging yield

$$\frac{d^2B}{dr^2} + \frac{1}{r}\frac{dB}{dr} - \frac{i\mu_0\omega}{\eta(1 + i\alpha)} B = 0 \tag{17}$$

Using equation (15) and changing variables from r to ξ where

$$\xi = \frac{r}{\delta}\left(\frac{-2i}{1 + i\alpha}\right)^{1/2} = \frac{r}{\delta}\frac{\sqrt{2}}{\left(1 + \alpha^2\right)^{1/4}} \exp\left(\frac{i\pi}{2} + \frac{i}{2}\cot^{-1}\alpha\right) \tag{18}$$

yield Bessel's equation of zero order

$$\frac{d^2B}{d\xi^2} + \frac{1}{\xi}\frac{dB}{d\xi} + B = 0 \tag{19}$$

The solution of equation (19) for B finite at $\xi = 0$ is

$$B = KJ_0(\xi) \tag{20}$$

Applying the boundary conditions $B = B_a$ at $r = a$ or $\xi = \xi_a$ yields

$$B = B_a \frac{J_0(\xi)}{J_0(\xi_a)} \tag{21}$$

To determine $\vec{E}$, equation (7) may be rewritten as

$$\frac{1}{r}\frac{d}{dr}(rE) = -i\omega B \tag{22}$$

where $\vec{E} = E\vec{\theta}$. Substituting equation (21) into equation (22), using equation (18), and simplifying yield

$$E = -i\omega\delta\left(\frac{-2i}{1 + i\alpha}\right)^{-1/2} \frac{1}{\xi}\frac{B_a}{J_0(\xi_a)} \int_0^{\xi} J_0(\xi)\xi\, d\xi \tag{23}$$

or

$$E = -i\omega\delta\left(\frac{-2i}{1 + i\alpha}\right)^{-1/2} \frac{J_1(\xi)}{J_0(\xi_a)} B_a \tag{24}$$

which may be written as

$$E = -\frac{\omega\delta}{\sqrt{2}}\left(1+\alpha^2\right)^{1/4} B_a \frac{J_1(\xi)}{J_0(\xi_a)} \exp\left(-\frac{i}{2}\cot^{-1}\alpha\right) \tag{25}$$

The variation of E and B with radial position is considered in detail in appendix B. The significance of two important limiting cases should be mentioned at this point, however. For $\alpha = 0$, that is, for high density plasmas where the electron inertia term in the Ohm's law is negligible, the solution reduces to that for the induction heating of a solid cylindrical rod (ref. 8). Hollister (ref. 9) has investigated this particular case as it applies to a diagnostic method for high-density plasmas. In this case, it is well known that the inward penetration distance of the electric and magnetic fields is the normal r-f skin depth δ. On the other hand, for low-density plasmas $\alpha \gg 1$ and from equation (18), it follows that, in the limiting case of very large α,

$$\xi \approx i\frac{a}{\delta}\left(\frac{2}{\alpha}\right)^{1/2} = ia\left(\frac{\mu_0 n_e q^2}{m_e}\right)^{1/2} = i\frac{\omega_p}{c}a \tag{26}$$

where

$$\omega_p \equiv \left(\frac{n_e q^2}{\epsilon_0 m_e}\right)^{1/2} \tag{27}$$

In this case, the penetration distance becomes c/ω_p, which is the characteristic attenuation distance for a transverse electromagnetic wave in a collisionless plasma when the wave frequency is much below the plasma frequency (ref. 6, p. 54).

Power Dissipated in Plasma

The solution for the power dissipated in the plasma can now be obtained by evaluating the real part of the complex Poynting vector at the surface $r = a$. When $r = a$ and $\xi = \xi_a$, the left side of equation (12a) becomes

$$-\frac{1}{\mu_0}\int_{S_{r=a}}\frac{1}{2}\left(\vec{E}\times\vec{B}^*\right)\cdot d\vec{S}=-\frac{1}{2\mu_0}\,2\pi a l E_a B_a^* \tag{28}$$

where l is the length of the plasma.

Substituting equation (25) into equation (28) results in

$$-\frac{1}{\mu_0}\int_{S_{r=a}}\frac{1}{2}\left(\vec{E}\times\vec{B}^*\right)\cdot d\vec{S}=\frac{1}{2}\,\frac{2\pi a l}{\mu_0}\,B_a^2\,\frac{\omega\delta}{\sqrt{2}}\left(1+\alpha^2\right)^{1/4}\frac{J_1(\xi_a)}{J_0(\xi_a)}\exp\left(-\frac{i}{2}\cot^{-1}\alpha\right) \tag{29}$$

Letting

$$\frac{J_1(\xi_a)}{J_0(\xi_a)}=\mathrm{Re}\left[\frac{J_1(\xi_a)}{J_0(\xi_a)}\right]+i\,\mathrm{Im}\left[\frac{J_1(\xi_a)}{J_0(\xi_a)}\right] \tag{30}$$

and noting that

$$\exp\left(-\frac{i\cot^{-1}\alpha}{2}\right)=\cos\left(\frac{\cot^{-1}\alpha}{2}\right)-i\sin\left(\frac{\cot^{-1}\alpha}{2}\right)$$

$$=\frac{1}{\sqrt{2}}\left\{\frac{\left[\left(1+\alpha^2\right)^{1/2}+\alpha\right]^{1/2}}{\left(1+\alpha^2\right)^{1/4}}-\frac{i\left[\left(1+\alpha^2\right)^{1/2}-\alpha\right]^{1/2}}{\left(1+\alpha^2\right)^{1/4}}\right\} \tag{31}$$

yield, for equation (29),

$$-\frac{1}{\mu_0}\int_{S_{r=a}}\frac{1}{2}\left(\vec{E}\times\vec{B}^*\right)\cdot d\vec{S}=2\pi a l\,\frac{B_a^2\omega\delta}{\mu_0^4}\left(\left[\left(1+\alpha^2\right)^{1/2}+\alpha\right]^{1/2}\mathrm{Re}\left[\frac{J_1(\xi_a)}{J_0(\xi_a)}\right]\right.$$

$$+\left[\left(1+\alpha^2\right)^{1/2}-\alpha\right]^{1/2}\mathrm{Im}\left[\frac{J_1(\xi_a)}{J_0(\xi_a)}\right]+i\left\{\left[\left(1+\alpha^2\right)^{1/2}+\alpha\right]^{1/2}\mathrm{Im}\left[\frac{J_1(\xi_a)}{J_0(\xi_a)}\right]\right.$$

$$\left.\left.-\left[\left(1+\alpha^2\right)^{1/2}-\alpha\right]^{1/2}\mathrm{Re}\left[\frac{J_1(\xi_a)}{J_0(\xi_a)}\right]\right\}\right) \tag{32}$$

By taking the real part of equation (32), the average power coupled to the plasma per unit surface area is

$$\overline{P} \equiv \frac{\overline{W}}{2\pi a l} = \frac{\omega\delta}{4}\frac{B_a^2}{\mu_0}\left\{\left[\left(1+\alpha^2\right)^{1/2}+\alpha\right]^{1/2}\mathrm{Re}\left[\frac{J_1(\xi_a)}{J_0(\xi_a)}\right]+\left[\left(1+\alpha^2\right)^{1/2}-\alpha\right]^{1/2}\mathrm{Im}\left[\frac{J_1(\xi_a)}{J_0(\xi_a)}\right]\right\} \tag{33}$$

Now, define a nondimensional power $\widetilde{P}$ as

$$\widetilde{P} \equiv \frac{\mu_0}{\omega a B_a^2}\frac{\left(1+\alpha^2\right)^{1/4}}{\left[\left(1+\alpha^2\right)^{1/2}-\alpha\right]^{1/2}}\overline{P} = \frac{\delta}{4a}\left(1+\alpha^2\right)^{1/4}\left\{\left[\left(1+\alpha^2\right)^{1/2}+\alpha\right]\mathrm{Re}\left[\frac{J_1(\xi_a)}{J_0(\xi_a)}\right]+\mathrm{Im}\left[\frac{J_1(\xi_a)}{J_0(\xi_a)}\right]\right\} \tag{34}$$

and the quantity h as

$$h \equiv \frac{\sqrt{2}\,a}{\delta\left(1+\alpha^2\right)^{1/4}} \tag{35}$$

Note that h is the magnitude of the complex argument ξ_a and is thus the ratio of radius to field penetration.

Combining equations (34) and (35) yields

$$\widetilde{P} = \frac{1}{2\sqrt{2}\,h}\left\{\left[\left(1+\alpha^2\right)^{1/2}+\alpha\right]\mathrm{Re}\left[\frac{J_1(\xi_a)}{J_0(\xi_a)}\right]+\mathrm{Im}\left[\frac{J_1(\xi_a)}{J_0(\xi_a)}\right]\right\} \tag{36}$$

where equation (18) becomes

$$\xi_a = h\exp\left(\frac{i\pi}{2}+\frac{i\cot^{-1}\alpha}{2}\right) \tag{37}$$

A plot of $\widetilde{P}$ against h with α as a parameter is given in figure 1. The cases $\alpha = 0$ (high-density plasma) and $\alpha \gg 1$ (low-density plasma) are shown by the curves, while some intermediate cases ($\alpha = 1, 3$) are indicated by data points. Figure 1 shows that $\widetilde{P}$ is independent of α for $\alpha \geq 3$ and that the solution for $\alpha \gg 1$ may be used

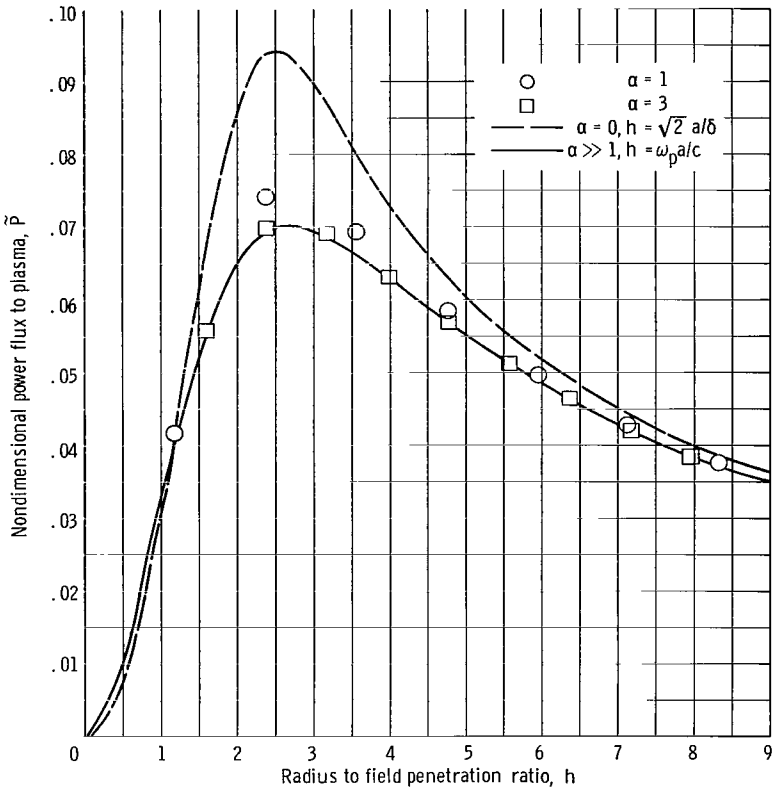

Figure 1. - Nondimensional power flux as function of radius to field penetration ratio with α as parameter.

as a very good approximation for these α values. This solution is shown in appendix C to be

$$\tilde{P} = \frac{1}{2\sqrt{2}} \left[\frac{I_1^2(h)}{I_0^2(h)} - \frac{I_2(h)}{I_0(h)} \right] \tag{38}$$

where the I(h)'s are the modified Bessel functions. In this case, h is a function of electron density only; that is,

$$h = \frac{\sqrt{2}\ a}{\delta\sqrt{\alpha}} = a\left(\frac{\mu_0 n_e q^2}{m_e}\right)^{1/2} = \frac{\omega_p a}{c} \tag{39}$$

Inductance of Plasma and Inductance Change of Radio-Frequency Coil

The average energy $\overline{U}$ stored in the plasma during a cycle is obtained by taking the imaginary part of equation (32) and dividing by 2ω (see eq. (12a)). Thus,

$$\overline{U} = \frac{B_a^2 \pi a l}{4\mu_0} \delta \left\{ \left[\left(1 + \alpha^2\right)^{1/2} + \alpha \right]^{1/2} \mathrm{Im}\left[\frac{J_1(\xi_a)}{J_0(\xi_a)}\right] - \left[\left(1 + \alpha^2\right)^{1/2} - \alpha \right]^{1/2} \mathrm{Re}\left[\frac{J_1(\xi_a)}{J_0(\xi_a)}\right] \right\} \tag{40}$$

The effect of this energy storage on the external circuit in an experiment is to reduce the observable inductance of the r-f coupling coil. Defining the inductance of the plasma such that

$$\frac{1}{2} L_p \overline{I^2} = \overline{U} \tag{13}$$

(see ref. 7, p. 202) and noting that $\overline{I^2} = I_m^2/2$ yield

$$L_p = \frac{\pi a l \delta B_a^2}{\mu_0 I_m^2} Y \tag{41}$$

where

$$Y = \left[\left(1 + \alpha^2\right)^{1/2} + \alpha \right]^{1/2} \mathrm{Im}\left[\frac{J_1(\xi_a)}{J_0(\xi_a)}\right] - \left[\left(1 + \alpha^2\right)^{1/2} - \alpha \right]^{1/2} \mathrm{Re}\left[\frac{J_1(\xi_a)}{J_0(\xi_a)}\right] \tag{42}$$

Consider the observable change in the coil inductance when the radius of the r-f coil b is larger than the plasma radius a. The observed change of inductance will be the change that occurs in the volume occupied by the plasma. When no plasma is present, the inductance associated with this volume is

$$L_{op} = \frac{\pi l B_a^2}{\mu_0 I_m^2} a^2 \tag{43}$$

The change of inductance when a plasma is present is, therefore,

$$\Delta L = L_{op} - L_p = \frac{\pi \ell B_a^2}{\mu_0 I_m^2} - \frac{\pi \ell \delta B_a^2}{\mu_0 I_m^2} aY \tag{44}$$

which may be rewritten as

$$\frac{\Delta L}{L_{op}} = 1 - \frac{\delta}{a} Y \tag{45}$$

The quantity $\Delta L/L_{op}$ (eq. (45)) is plotted as a function of h with α as a parameter in figure 2. It is again seen from this figure that the α dependence is not important for $\alpha \geq 3$ and, therefore, the solution for $\alpha >> 1$ may be used for these α values. In this case, the observable change in coil inductance will be a function of electron density only and is given by (see appendix C)

$$\Delta L = L_{op}\left[1 - \frac{2}{h}\frac{I_1(h)}{I_0(h)}\right] \tag{46}$$

It should be noted, however, that the fractional change in inductance, which is measured experimentally, is $\Delta L/L_T$, where L_T is the total inductance of the r-f coil. Consequently, even though ΔL is a large fraction of L_{op}, the measurement may be quite difficult if it is a small portion of L_T.

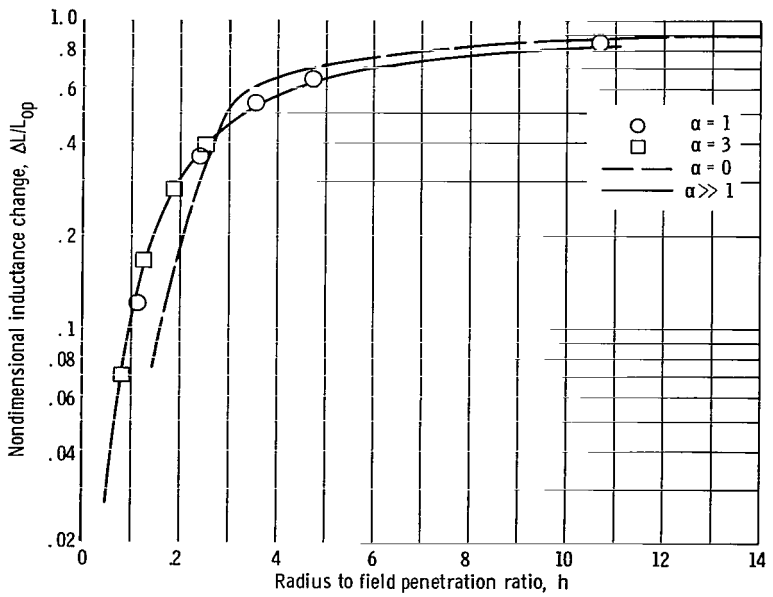

Figure 2. - Nondimensional inductance change as function of radius to field penetration ratio.

EXPERIMENT

Apparatus

A photograph of the r-f induction heater in operation is shown in figure 3. Figure 4 is a schematic diagram of the apparatus. The test chamber consists of two concentric glass funnels with cooling air passing between them. Two glass to metal seals are attached to the top of the inner funnel and have conventional O-ring fittings welded to the metal sections. Helium gas was introduced into the system through a quartz tube inserted in the center O-ring fitting. The second fitting was used as an entry port for diagnostic devices.

A Faraday shield, consisting of a series of insulated vertical copper wires with a common ground, was located between the funnels to ensure operation in the inductive mode. A small confining direct-current field of 20 to 30 gauss (20×10^{-4} to 30×10^{-4} T) is supplied by the direct-current field coils in a magnetic mirror geometry. This field increases the stability of the discharge and allows continuous operation for long periods of time.

The 7.7-centimeter-diameter r-f coil is a 4-turn silver-plated copper coil of length 7.5 centimeter. Magnetic-field measurements were made with a single turn magnetic-

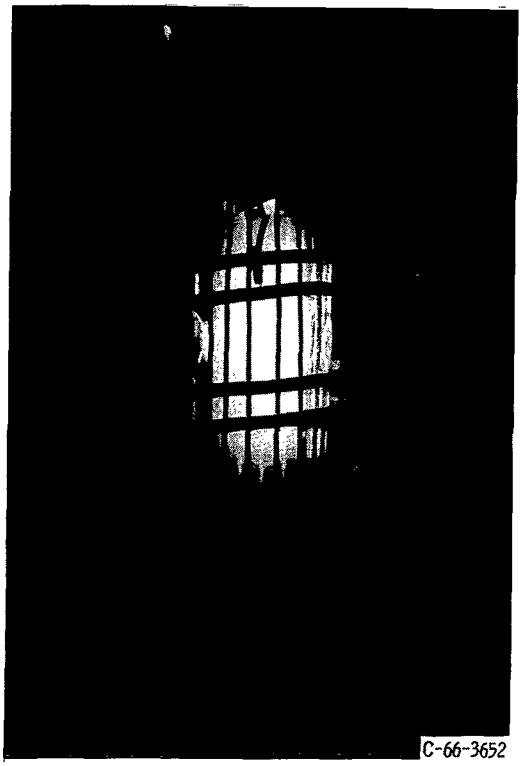

Figure 3. - Radio-frequency induction heater in operation.

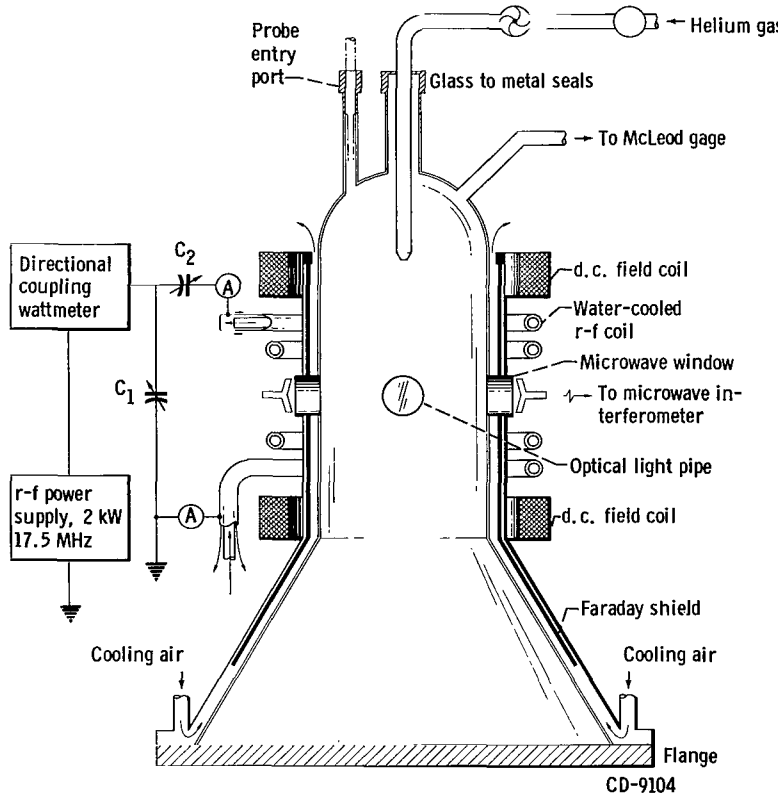

Figure 4. - Schematic of test apparatus.

field probe. This probe was located on the wall of the inner funnel; hence, it measured an effective average of the r-f field over the cross sectional area. Measurements at various axial positions showed that the r-f magnetic field was approximately constant (±10 percent) over the coil length. Both the direct-current and r-f coils were water cooled. The r-f power is supplied by a 2-kilowatt, 17.5-megahertz transmitter. The capacitors C_1 and C_2 are calibrated, variable vacuum capacitors.

A microwave interferometer is used to measure electron density. Two microwave windows were positioned on the sides of the inner funnel. A fiber optics light pipe was used to transmit the helium spectral line radiation to a 0.5-meter Ebert monochromator. The entire system was exhausted into a 32-inch (0.813 m) oil diffusion pump.

Electrical Instrumentation and Determination of Plasma Properties

The electrical properties needed to compare the experimental data with the theory are the power coupled to the plasma, the current in the r-f coil, the change of inductance of the r-f coil, and the plasma electron density and resistivity.

Power measurement. - The power coupled to the plasma is measured by using a commercial directional coupling wattmeter. This wattmeter measures the forward power into the matching network and load coil when the system is tuned for zero reflected power and its impedance matches the transmitter impedance of 50 ohms.

Coil current and inductance measurements. - The values of the coil current and inductance change are obtained from direct measurements of the circuit parameters. The equivalent circuit for the impedance matching network, coil, and plasma system is shown in figure 5.

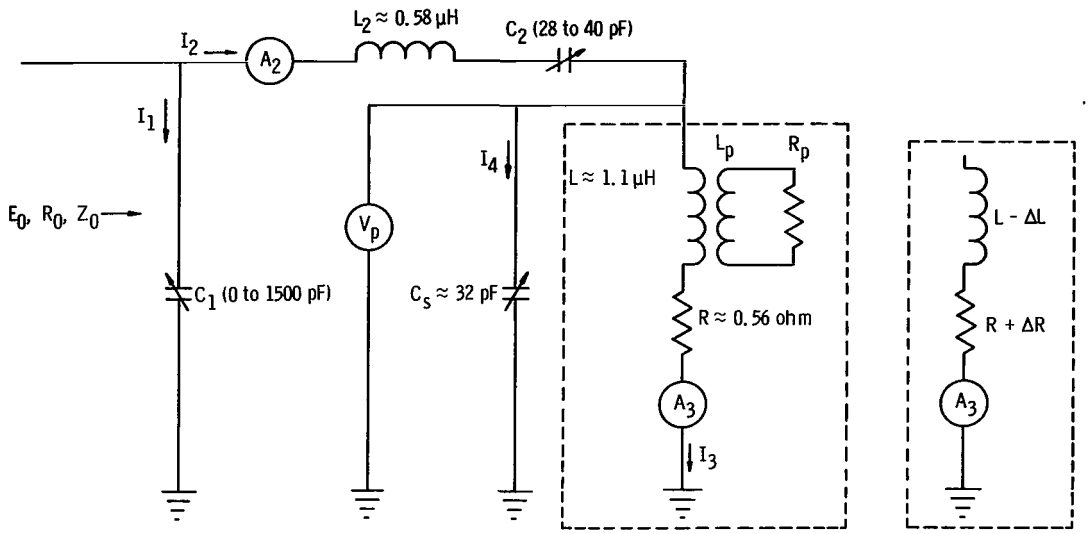

Figure 5. - Equivalent circuit diagram for impedance matching network, radio-frequency coil and plasma system.

In this figure, E_0 is the applied voltage and R_0 is the total impedance when the system is tuned for zero reflected power and equals the transmitter impedance of 50 ohms. C_1 and C_2 are calibrated variable capacitors and L_2 is the inductance of the strap connecting C_1 and C_2 plus the lead inductance of the coil. L is the coil inductance plus the lead to ground inductance, R is the coil resistance, and C_s is the stray capacitance. This capacitance is a result of the distributed capacitance of the coil, the Faraday shield, and the voltmeter. However, because the effect of this capacitance on the circuit measurements is the main interest, it is considered as a lumped capacitor across the r-f coil. The plasma inductance and resistance are represented by L_p and R_p, respectively. The ammeters A_2 and A_3 measure the rms values of the current I_2 and the coil current I_3, while the voltmeter V_p measures the peak voltage across the L-R-C_s network. For a high Q circuit, the change in inductance may be obtained directly from the V_p and I_3 measurements and the relation

$$L - \Delta L = \frac{V_p}{\sqrt{2}\, I_3 \omega} \tag{47}$$

However, because of some inconsistencies in the voltage measurements (see appendix D), an alternate method for determining ΔL, which did not require voltage measurements, was also employed. The net reactance of the $L - \Delta L$, $R + \Delta R$, C_s portion of the circuit is inductive, and this portion may be replaced by an apparent resistance R_a and apparent inductance L_{ap}. For a high Q circuit, the magnitude of the impedance of this portion of the circuit is, to a very good approximation, that of the apparent inductance (see Swett, ref. 10); that is,

$$Z_{eff} = \frac{\left(R^2 + \omega^2 L^2\right)^{1/2}}{\left[\omega^2 C_s^2 R^2 + \left(\omega^2 L C_s - 1\right)^2\right]^{1/2}} \approx \omega \left(\frac{L}{1 - \omega^2 L C_s}\right) \approx \omega L_{ap} \tag{48}$$

Therefore, the voltage V_p is also given by

$$V_p = \sqrt{2}\, I_2 \omega L_{ap} \tag{49}$$

and using equation (47) yields for $L - \Delta L$

$$L - \Delta L = \frac{I_2}{I_3} L_{ap} \tag{50}$$

At resonance conditions ($Z_0 = R_0 = 50$ ohms), L_{ap} may be obtained from the C_1 and C_2 readings using the relation

$$L_{ap} = \frac{C_1 R_0^2}{\omega^2 C_1^2 R_0^2 + 1} + \frac{1}{\omega^2 C_2} - L_2 \tag{51}$$

or using the values $R_0 = 50$ ohms and $\omega = 1.099 \times 10^8$ per second results in

$$L_{ap} = \frac{2.5 \times 10^{-3}\, C_1}{3.02 \times 10^{-5}\, C_1^2 + 1} + \frac{82.78}{C_2} - L_2 \tag{52}$$

where L_{ap} and L_2 are in microhenries if C_1 and C_2 are given in picofarads.

In order to ensure the validity of the current and voltage measurements and the values of the circuit parameters, it was necessary to conduct a detailed circuit check (presented in appendix D).

Plasma property measurements. - The electron density was obtained by measuring the phase change of a microwave beam when it passed through the plasma. This measurement was accomplished by using the 39.5 gigahertz microwave interferometer that is shown schematically in figure 6. The data was reduced following the method of Kuhns (ref. 11).

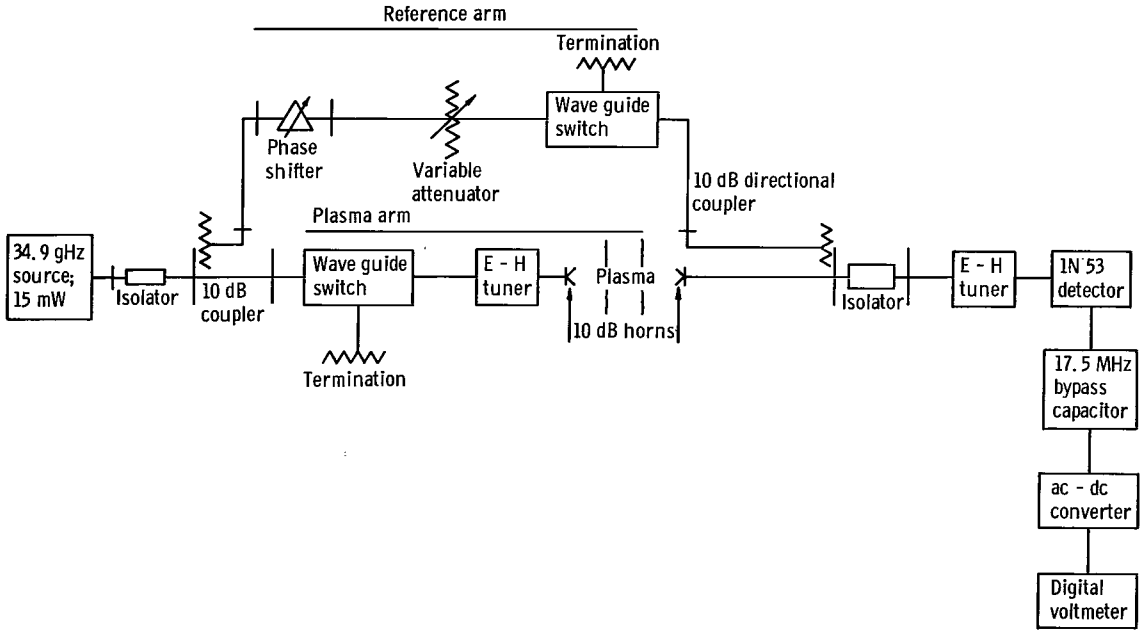

Figure 6. - Schematic diagram of microwave interferometer.

The plasma resistivity is obtained from measurements of the pressure, electron temperature, and electron density and by using the relations given in appendix E. The electron temperature is obtained by using the spectroscopic technique refined in reference 12, which is also discussed in more detail in appendix B.

Experimental Procedure

The procedure followed was to first obtain data for the system with no plasma present. In these tests, the impedance matching network was tuned for zero reflected power and the forward power was measured for a series of coil currents. Once these measurements were obtained, the desired helium gas flow was set and the r-f voltage was then

increased until a discharge was initiated. Once the plasma was obtained, the match network was again tuned to zero reflected power and the desired coil current was obtained by varying the r-f voltage. The system was then allowed to run for a few minutes, and, if no changes in the reflected power or coil current were observed, the data were taken.

The quantities measured for each data point were the pressure, forward power, coil current, direct field current, transmitter-plate voltage and current, series and shunt capacitances, spectral line intensities, microwave interferometer measurements, and the various circuit voltages and currents needed to determine the inductance change and other circuit parameters.

Experimental Data

Some typical experimental data are presented in table I. In obtaining the experimental data, the power coupled to the plasma $\overline{P}_g$, the pressure, electron density, coil current, and electron temperature were found to be interdependent quantities. Because of the limitations on the amount of power (0 to 1000 W) that could be coupled to the plasma and the range of electron densities (1×10^{16} to 5×10^{18} m^{-3}) that could be measured, a detailed parametric study of these quantities was not made. However, a typical variation of these quantities with pressure at a constant coil current is shown in figure 7. This figure shows that the electron density and the power coupled to the plasma increase almost linearly with pressure. The electron temperature decreased with increasing pressure, a result which is in agreement with the results of Pell for low pressures

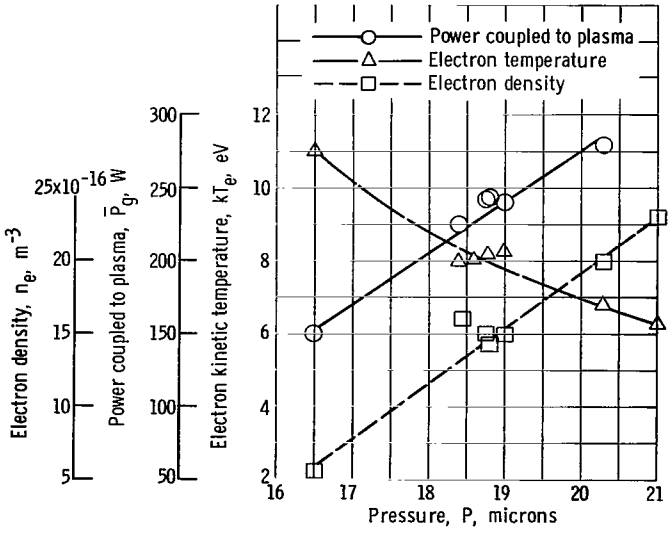

Figure 7. - Typical variation of power coupled to plasma, electron temperature and electron density with pressure at a constant coil current.

TABLE I. - DATA TABLE

Root mean square coil current, A	Forward power, W	Total power coupled to plasma, $\overline{P}_g$, W	Power transfer efficiency, percent	Electron kinetic temperature, kT_e, eV	Electron density, n_e, m^{-3}	Neutral density, n_o, m^{-3}	Fraction ionized, f_i	Plasma resistivity, η, ohm-m	$P_g/I_m^2\eta$, m^{-1}	Inductance change, ΔL, μH	
										Method 1	Method 2
14	219	108	50	8.8	6.7×10^{16}	5.34×10^{20}	1.25×10^{-4}	19×10^{-3}	14.5	0.03	-----
14.8	247	127	51	8.7	7.1	5.05	1.41	17	17	.039	0.043
15.6	289	152	53	9.1	10.2	5.0	2.04	11	27.9	.031	.036
16.4	335	182	55	8.4	11.2	4.97	2.25	10	33.2	.043	.027
16.9	490	325	66	4.0	36.7	7.39	4.96	4.8	119	.045	.068
17.4	423	253	60	7.3	17.1	5.42	3.15	7.0	58	-----	.018
18	390	195	50	---	12	----	----	---	-----	.029	.014
18	364	169	47	---	6.5	----	----	---	-----	.018	.01
18	474	279	59	---	19.5	----	----	---	-----	.036	.033
18	510	315	62	---	22.8	----	----	---	-----	.036	.040
18	575	380	66	---	35.5	----	----	---	-----	.051	.051
18	620	423	68	---	40	----	----	---	-----	.047	.067
18.1	435	240	55	8.5	14.9	5.0	2.98	8	48	.036	.023
18.1	594	404	68	4.0	42.8	7.4	5.8	4.3	144	.056	.070
18.3	474	279	59	6.8	19.9	5.34	3.72	6.6	63	.030	.025
19.2	505	300	60	8.3	17.1	4.79	3.56	6.5	63	.045	.040
19.7	705	480	68	4.0	49	7.08	6.92	3.4	182	.066	.068
20	548	323	59	8.1	18.9	4.73	4.0	6.0	71	.044	.052
20	594	372	63	6.5	24	5.4	4.45	5.4	86	.045	.049
20	621	396	64	6.1	26.5	5.58	4.75	5.2	95	.052	.048
20	715	475	67	---	33.2	----	----	---	-----	.036	.064
20	760	520	69	---	44	----	----	---	-----	.046	.068
20	895	655	73	---	42.5	----	----	---	-----	.042	.062
20.1	588	363	62	6.7	23	5.23	4.4	5.4	83	.043	.036
20.5	622	382	62	6.7	19.5	5.26	3.7	6.6	69	.047	.070
20.6	676	435	64	5.9	24.1	5.65	4.26	5.6	92	.052	.062
21.2	715	452	63	6.0	28.1	5.39	5.21	4.5	112	.045	.047
21.8	695	425	61	7.6	23.8	4.66	5.10	4.3	104	.043	.042
22.1	798	523	66	6.0	32	5.34	6.0	4.0	134	.040	.063

(private communication from K. M. Pell of University of Florida). The power transfer efficiencies defined as the power coupled to the plasma divided by the forward power are also listed in table I. These efficiencies were from 47 to 73 percent.

COMPARISON OF THEORETICAL AND EXPERIMENTAL RESULTS

The solution for the nondimensional power per unit area coupled to the plasma for the case $\alpha >> 1$ was given by equation (38) as

$$\tilde{P} = \frac{1}{2\sqrt{2}} \left[\frac{I_1^2(h)}{I_0^2(h)} - \frac{I_2(h)}{I_0(h)} \right]$$

where $h = \omega_p a/c = 1.88 \times 10^{-7} a\sqrt{n_e}$; therefore, $\tilde{P}$ is a function of n_e only.

The dimensional power coupled to the plasma per unit area is obtained from equation (34) and is

$$\overline{P} = \frac{B_a^2 \omega a}{\mu_0} \frac{\left[\left(1 + \alpha^2\right)^{1/2} - \alpha \right]^{1/2}}{\left(1 + \alpha^2\right)^{1/4}} \tilde{P}(n_e) = \frac{\sqrt{2}\ B_a^2 \omega a}{\mu_0} \sin\left(\frac{\cot^{-1}\alpha}{2}\right) \tilde{P}(n_e) \tag{53}$$

Noting that $\sin\left(\frac{\cot^{-1}\alpha}{2}\right) \approx \frac{1}{2\alpha}$ for $\alpha >> 1$ yields for $\overline{P}$

$$\overline{P} = \frac{B_a^2 \omega a}{\sqrt{2}\ \mu_0 \alpha} \tilde{P}(n_e) \tag{54}$$

The total power coupled to the plasma is, therefore,

$$\overline{P}_g = 2\pi a l \overline{P} = \frac{2\pi a^2 l \omega}{\sqrt{2}\ \mu_0 \alpha} B_a^2 \tilde{P}(n_e) \tag{55}$$

In order to compare the results of this analysis with the experimental data, the following substitutions are made:

$$\alpha = \frac{m_e \omega}{\eta n_e q^2}$$

and

$$B_a^2 = \frac{C_B^2 \mu_0^2 N^2 I_m^2}{l^2}$$

where C_B is a correction factor for the short solenoid used in the experiment. The value of C_B was obtained from measurements of the field produced by the coil at different axial positions with magnetic-field probes. The following values of the experimental constants were used:

Plasma radius, a, m	0.024
Length of plasma, l, m	0.075
Correction factor for short solenoid, C_B^2	0.233
Applied frequency, ω, sec^{-1}	1.099×10^8
Number of turns in coil, N	4

Substitution of these values and the quantities α and B_a^2 into equation (55) yields

$$\overline{P}_g = 4.52 \times 10^{-15} I_m^2 \eta n_e \widetilde{P}(n_e) \tag{56}$$

or

$$\frac{\overline{P}_g}{I_m^2 \eta} = 4.52 \times 10^{-15} n_e \widetilde{P}(n_e) \tag{57}$$

The assumption $\alpha >> 1$ produces a maximum error in $\overline{P}$ of 4 percent if $\alpha = 3$ and 2 percent if $\alpha = 4$. Most of the α values obtained experimentally are $\alpha \geq 4$; therefore, the experimental results are compared with the theory for $\alpha >> 1$. In this case, ΔL is given by (see appendix C)

$$\Delta L = L_{op} \left[1 - \frac{2}{h} \frac{I_1(h)}{I_0(h)} \right] \tag{46}$$

where L_{op} is defined by equation (43) and is calculated to be 0.113 microhenry.

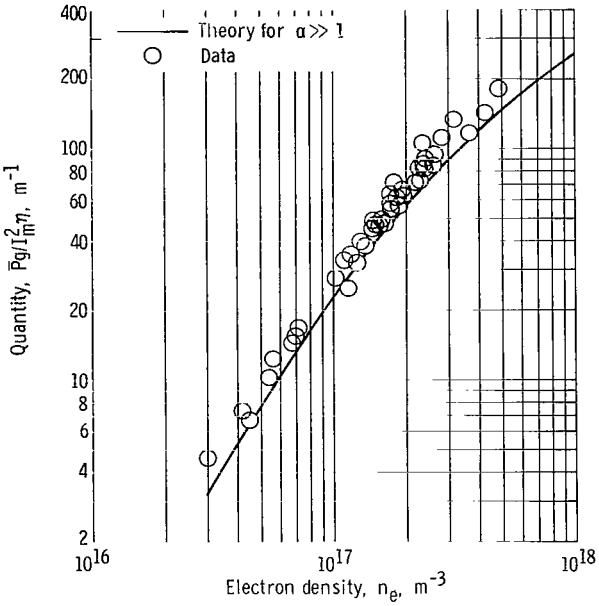

Figure 8. - Comparison of experimental and theoretical results for power coupled to plasma (see eq. (57)) for $\alpha \gg 1$.

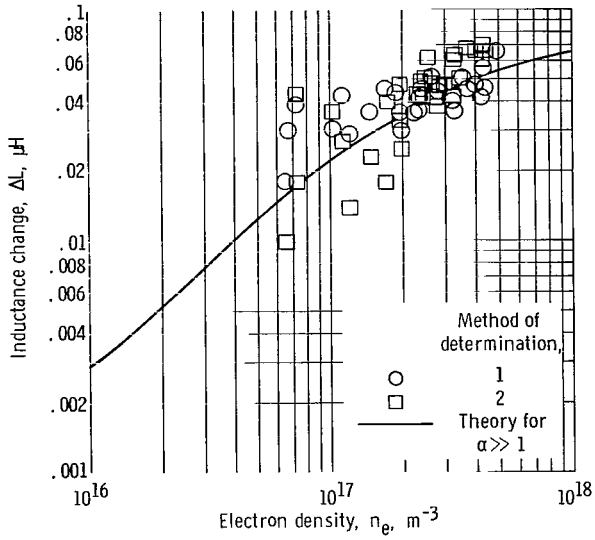

Figure 9. - Comparison of experimental and theoretical results of inductance change for $\alpha \gg 1$.

A comparison of the theoretical (eqs. (57) and (46)) and experimental results is shown in figures 8 and 9. Reasonably good agreement is evident between theory and experiment. The experimental data for the power coupled to the plasma are slightly higher (≈10 percent) than the theory predicts, but they definitely exhibit the same dependence on electron density that is predicted by the theory. One reasonable explanation for the slight discrepancy in magnitude could be an error in the determination of the plasma volume. The plasma radius was taken to be the inner radius of the inner funnel, and the plasma length was taken to be the length of the r-f coil. In reality, the plasma did fill the coil and inner funnel but there was also a plume of plasma above the r-f coil. The tendency would be to underestimate slightly the plasma volume. This difference could easily account for the slight discrepancy between the theoretical and experimental results. Another possible reason for this discrepancy could be in the treatment of the electron density. In the theory, the spatially dependent electron density was replaced by a uniform effective electron density. The microwave interferometer measures an average electron density across the diameter of the plasma. However, this averaged electron density is not necessarily the same as the assumed effective electron density.

The direct-current field did not affect the data since the system was not operated at any of the resonant frequencies for the plasma constituents. Data taken with and without the direct-current field fell on the same curve. However, the direct-current field permitted steady-state operation over a wider range of parameters.

The inductance change data (fig. 9) also agreed with the theory, although there is a

large amount of scatter in the data. This scatter is understandable, however, in view of the difficulties entailed in measuring such small inductance changes. It was for this reason that two methods of measuring these changes were employed. An experiment designed such that a large change in inductance is expected would probably have much less scatter.

CONCLUDING REMARKS

An experimental and theoretical investigation of radio-frequency induction heating and production of plasmas has been carried out. A linearized analysis was performed for the coupling of a solenoidal radio-frequency magnetic field with a steady cylindrical plasma. The good agreement obtained between the experimental and theoretical results indicates that the linearized analysis serves as a very good approximation for predicting the power coupled to the plasma and inductance change as a function of the plasma properties. The fact that the inductance change is a function of electron density only for low-pressure plasmas indicates that the measured inductance change may be used to measure the average plasma electron density.

Lewis Research Center,
National Aeronautics and Space Administration,
Cleveland, Ohio, April 25, 1967,
120-26-03-04-22.

APPENDIX A

SYMBOLS

A_2, A_3	ammeters
A'	$2.3 \log_{10} d'/c$
a	plasma radius, m
B	magnetic-flux intensity, T
B'	$0.366 (1 - 2.5/N + 3.8/N^2)$
b	coil radius, m
C	capacitance, pF
C_B	correction factor for magnetic field produced by short coil
C_c	correction factor used in calculating coil inductance, defined by eq. (C3)
C_s	stray capacitance, pF
C_1, C_2	calibrated variable capacitators
c	winding pitch of coil
D	electric displacement, c/m^2
d'	diameter of coil tubing, m
E	electric-field strength, V/m
E_0	applied voltage, V
f_i	fraction ionized
H	magnetic-field intensity, A/m
h	nondimensional radius to field penetration ratio (see eq. (35))
I	electric current, A
Im	imaginary part of
$I_n(h)$	modified Bessel function of order n and argument h
I_2	current through C_2, A
I_3	coil current, A
$J_n(\xi)$	Bessel function of order n and argument ξ

$\mathcal{J}$	ratio of rms magnitude of magnetic field at some radial position r to that at boundary r = a (eq. (B4))
$\mathcal{J}_1$	ratio of rms magnitude of electric field at some radial position r to that at boundary r = a (eq. (B12))
j	current density, A/m^2
K	constant defined by eq. (20)
K_n	correction factor for short coils defined by eq. (C2)
k	Boltzmann constant, 1.3805×10^{-23} $J/^oK$
kT_e	electron kinetic temperature, eV
L	inductance, μH
L_0	coil inductance, μH
L_{op}	inductance of plasma volume when no plasma is present, μH
L_p	plasma inductance, μH
L_2	inductance of strap used to connect C_1 and C_2 plus lead inductance of coil, μH
ℓ	length of plasma, m
$M_n(h)$	modulus of Kelvin functions of order n and argument h
m_e	electron rest mass, 9.108×10^{-31} kg
N	number of turns in coil
n_e	electron density, m^{-3}
n_0	neutral density, m^{-3}
$\overline{P}$	average flux to plasma during cycle, $\overline{W}/(2\pi a\ell)$, W/m^2
$\overline{P}_g$	total power coupled to plasma, W
$\tilde{P}$	nondimensional power defined by eq. (34)
p'	pressure, N/m^2 or μm
Q	$\omega L/R$
q	electron charge, 1.602×10^{-19} C
R	resistance, ohm
R_a	apparent resistance, ohm
Re	real part of

R_o total impedance when system is tuned for zero reflected power, 50 ohms

R_p plasma resistance, ohm

r radial coordinate

S surface area, m^2

T temperature, ^oK

T_0 neutral temperature in test chamber

T_0' neutral temperature in McLeod gage

t time, sec

$\overline{U}$ average reactive energy in plasma during cycle

$\overline{U}_{ke}$ average drift kinetic energy of electrons during cycle

$\overline{U}_M$ average magnetic energy during cycle

V volume, m^3

V_p peak voltage, V

v velocity, m/sec

v_e electron velocity, m/sec

$\overline{W}$ average resistive power coupled to plasma during cycle (see eq. (12b))

X reactance, ohm

Y defined by eq. (39)

Z impedance

Z_{eff} effective impedance of L-R-C_s portion of circuit

z axial coordinate

α dimensionless coordinate defined as ratio of r-f field frequency to collision frequency

β $\tan^{-1}\left[rhI_1(rh/a)/(2a\alpha I_0(rh/a)\right]$, see eq. (B8)

β' $\tan^{-1}\left[hI_1(h)/2\alpha I_0(h)\right]$, see eq. (B8)

γ $\tan^{-1}\left[2a\alpha I_1(rh/a)/rhI_2(rh/a)\right]$, see eq. (B16)

γ' $\tan^{-1}\left[2\alpha I_1(h)/hI_2(h)\right]$, see eq. (B16)

δ normal r-f skin depth, $(2\eta/\mu_0\omega)^{1/2}$

ϵ_0 dielectric constant of free space, F/m

η plasma resistivity, ohm-m

η_{ea} resistivity due to electron-atom collisions, ohm-m

η_{ei} resistivity due to electron-ion collisions, ohm-m

θ azimuthal coordinate

$\theta_n(h)$ phase angle of Kelvin functions of order n and argument h

Λ $12\pi(\epsilon_0 kT_e)^{3/2}/q^3 n_e^{1/2}$

μ_0 magnetic permeability of free space, H/m

ν_c total electron collision frequency, sec^{-1}

ν_{ea} electron-atom momentum transfer collision frequency, sec^{-1}

ν'_{ea} ν_{ea}/n_0, m^3/sec

ξ dimensionless variable defined as $(r/\delta)\left[-2i/(1 + i\alpha)\right]^{1/2}$

ρ ratio of radius to r-f skin depth, a/δ

$\sigma_{m_{el}}$ total momentum transfer cross section due to elastic collisions, m^2

τ time between electron collisions or total electron collision time, sec

φ $\tan^{-1} X_2/R_a$

Ψ electron kinetic energy, eV

ω applied frequency, rad/sec

ω_r resonant frequency of L-C network, rad/sec

Subscripts:

a evaluated at radial position r = a

ap apparent

m maximum value

Superscripts:

$\bar{}$ time averaged value over cycle

* complex conjugate

APPENDIX B

RADIAL PENETRATION OF MAGNETIC-FLUX DENSITY AND ELECTRIC-FIELD STRENGTH

In this appendix, the variations of B and E with radial position are investigated, and tables and plots of these variations are presented.

Solutions for Magnetic-Flux Intensity

General solution. - Including the time dependence, the solution for B is given by (see eq. (21))

$$B = B_a \mathrm{Re}\left[\frac{J_0(\xi)}{J_0(\xi_a)} e^{i\omega t}\right] \tag{B1}$$

where

$$\xi = \frac{r}{\delta} \frac{\sqrt{2}}{\left(1 + \alpha^2\right)^{1/4}} \exp\left(\frac{i\pi}{2} + \frac{i \cot^{-1}\alpha}{2}\right) = \frac{r}{a} h \exp\left(\frac{i\pi}{2} + \frac{i \cot^{-1}\alpha}{2}\right)$$

and

$$\xi_a = \frac{a}{\delta} \frac{\sqrt{2}}{\left(1 + \alpha^2\right)^{1/4}} \exp\left(\frac{i\pi}{2} + \frac{i \cot^{-1}\alpha}{2}\right) = h \exp\left(\frac{i\pi}{2} + \frac{i \cot^{-1}\alpha}{2}\right)$$

The quantity $J_0(\xi)/J_0(\xi_a)$ is a complex number which may be written in the polar form

$$\frac{J_0(\xi)}{J_0(\xi_a)} = \mathscr{f} e^{i\varphi} \tag{B2}$$

Equation (B1) then becomes

$$B = B_a \mathscr{f} \mathrm{Re}\left[e^{i(\omega t + \varphi)}\right] = B_a \mathscr{f} \cos(\omega t + \varphi) \tag{B3}$$

Taking the root mean square value yields

$$\frac{B_{rms}}{(B_a)_{rms}} = \mathcal{J} \tag{B4}$$

Therefore, the ratio of the root mean square magnitude of B at some radial position r to that at the boundary r = a is given by $\mathcal{J}$, and the phase difference between the two is given by φ.

Solutions when $\alpha = 0$ and $\alpha >> 1$. - When $\alpha = 0$,

$$\xi = \frac{r}{a} hi^{3/2}$$

$$\xi_a = hi^{3/2}$$

and

$$\frac{J_0(\xi)}{J_0(\xi_a)} = \frac{M_0\left(\frac{r}{a} h\right)}{M_0(h)} \exp\left[i\theta_0\left(\frac{r}{a} h\right) - i\theta_0(h)\right] \tag{B5}$$

where M_0 and θ_0 are the modulus and phase, respectively, of the Kelvin functions. Therefore, when $\alpha = 0$,

$$\mathcal{J} = \frac{M_0\left(\frac{r}{a} h\right)}{M_0(h)}$$

and

$$\varphi = \theta_0\left(\frac{r}{a} h\right) - \theta_0(h)$$

When $\alpha >> 1$,

$$\xi = \frac{r}{a} hie^{i/2\alpha}$$

and

$$\xi_a = hie^{i/2\alpha}$$

It is also shown in appendix C that, for $\alpha >> 1$,

$$J_0(\xi) = I_0\left(\frac{r}{a}h\right) + \frac{rh}{2a\alpha}\, iI_1\left(\frac{r}{a}h\right) \tag{B6}$$

and

$$J_0(\xi_a) = I_0(h) + \frac{h}{2\alpha}\, iI_1(h) \tag{B7}$$

Therefore, $J_0(\xi)/J_0(\xi_a)$ in polar form is, for $\alpha >> 1$,

$$\frac{J_0(\xi)}{J_0(\xi_a)} = \frac{\left[I_0^2\left(\frac{r}{a}h\right) + \left(\frac{rh}{2a\alpha}\right)^2 I_1^2\left(\frac{r}{a}h\right)\right]^{1/2}}{\left[I_0^2(h) + \left(\frac{h}{2\alpha}\right)^2 I_1^2(h)\right]^{1/2}} e^{i(\beta-\beta')} = \mathcal{J} e^{i(\beta-\beta')} \tag{B8}$$

where

$$\beta = \tan^{-1}\left[\frac{rhI_1\left(\frac{r}{a}h\right)}{2a\alpha I_0\left(\frac{r}{a}h\right)}\right]$$

and

$$\beta' = \tan^{-1}\left[\frac{hI_1(h)}{2\alpha I_0(h)}\right]$$

For $\alpha >> 1$, and from equation (B8),

$$\mathcal{J} = \frac{I_0\left(\frac{r}{a}h\right)}{I_0(h)}$$

and

$$\varphi = \beta - \beta'$$

Solutions for Electric-Field Strength

General solution. - Evaluating equation (25) at $r = a$ yields, for E including the time dependence,

$$E = E_a \mathrm{Re}\left[\frac{J_1(\xi)}{J_1(\xi_a)} e^{i\omega t}\right] \tag{B9}$$

Following the procedure used in the preceding discussion for the magnetic field results in

$$\frac{J_1(\xi)}{J_1(\xi_a)} = \mathcal{J}_1 e^{i\varphi_1} \tag{B10}$$

and

$$E = E_a \mathcal{J}_1 \cos(\omega t + \varphi_1) \tag{B11}$$

or

$$\frac{E_{rms}}{(E_a)_{rms}} = \mathcal{J}_1 \tag{B12}$$

Therefore, the ratio of the rms magnitude of E at some radial position r to that at the boundary $r = a$ is given by $\mathcal{J}$ and the phase difference between the two is φ_1.

Solutions when $\alpha = 0$ and $\alpha \gg 1$. - Letting $\alpha = 0$ and using the results of the first section of this appendix reveal that

$$\mathcal{J}_1 = -\frac{M_1\left(\frac{r}{a} h\right)}{M_1(h)} \tag{B13a}$$

and

$$\varphi_1 = \theta_1\left(\frac{r}{a} h\right) - \theta_1(h) \tag{B13b}$$

When $\alpha \gg 1$, it is shown in appendix C that

$$J_1(\xi) = e^{i/2\alpha}\left[iI_1\left(\frac{r}{a}h\right) - \frac{rh}{2a\alpha} I_2\left(\frac{r}{a}h\right)\right] \tag{B14}$$

and

$$J_1(\xi_a) = e^{i/2\alpha}\left[iI_1(h) - \frac{h}{2\alpha} I_2(h)\right] \tag{B15}$$

Therefore, in polar form,

$$\frac{J_1(\xi)}{J_1(\xi_a)} = \frac{\left[I_1^2\left(\frac{r}{a}h\right) - \left(\frac{rh}{2a\alpha}\right)^2 I_2^2\left(\frac{r}{a}h\right)\right]^{1/2}}{\left[I_1^2(h) - \left(\frac{h}{2\alpha}\right)^2 I_2^2(h)\right]^{1/2}} e^{i(\gamma-\gamma')} \tag{B16}$$

where

$$\gamma = \tan^{-1}\left[\frac{2a\alpha I_1\left(\frac{r}{a}h\right)}{rhI_2\left(\frac{r}{a}h\right)}\right]$$

and

$$\gamma' = \tan^{-1}\left[\frac{2\alpha I_1(h)}{hI_2(h)}\right]$$

For $\alpha >> 1$, equation (B16) yields

$$\mathcal{J}_1 = \frac{I_1\left(\frac{r}{a}h\right)}{I_1(h)} \tag{B17a}$$

$$\varphi_1 = \gamma - \gamma' \tag{B17b}$$

Tabulation and Use of Results for Radial Variation of Magnetic-Flux Density and Electric-Field Strength

Numerical values of the rms magnetic- and electric-field ratios $\mathcal{J}$ and $\mathcal{J}_1$, respectively, are presented in table II as functions of r/a, h, and α. The values for the phase angles φ and φ_1 are given in table III. In table III, it is understood that the fields in the plasma lag behind those at the boundary r = a and the absolute values of the phase angles are given.

In table II, results are presented for $\alpha = 0$, 1, 2, and $\alpha \gg 1$ only because the $\alpha \gg 1$ solution is good for $\alpha \geq 3$. When using results of this type the reader is generally interested in plots of the radial variation of the fields ($\mathcal{J}$, $\mathcal{J}_1$) for a given r-f skin depth and various α values. These results may be obtained from the data presented in table II. The manner in which the data are presented in table II is advantageous in that the data encompass a wide range of δ and α values. Letting the ratio of the radius to the r-f skin depth be ρ (i.e., $\rho = a/\delta$) yields for h

$$h = \frac{\sqrt{2}\,\rho}{\left(1 + \alpha^2\right)^{1/4}} \tag{B18}$$

If $\mathcal{J}$ and $\mathcal{J}_1$ are plotted as a function of h with r/a as a parameter for fixed α values of 0, 1, 2, and $\alpha \gg 1$ the desired information may be obtained directly from these plots. One merely chooses the desired ρ value and calculates the h for each α needed. The variations of $\mathcal{J}$ and $\mathcal{J}_1$ with r/a are obtained from the family of curves for the chosen α. An example of the type of results obtained is shown in figure 10 for $\rho = 10$.

The data for the phase angles φ and φ_1 are presented in table III. The phase angles depend on α even when $\alpha \gg 1$; therefore, these results are presented for α values of 0, 1, 2, 3, 5, 25, and 100. In order to obtain data for a constant ρ value, the same technique used for the $\mathcal{J}$ and $\mathcal{J}_1$ quantities is followed (i.e., a family of curves of φ and φ_1 as a function h is obtained with r/a as a parameter for each α). If data for α values not included in table III are needed, the data in table III must be used to obtain auxiliary plots of φ and φ_1 as a function of α with h as a parameter for each r/a. A plot of the phase-angle variations with r/a and α for $\rho = 10$ is presented in figure 11.

TABLE II. - VARIATION OF ROOT MEAN SQUARE MAGNITUDES OF MAGNETIC-FLUX AND ELECTRIC-FIELD STRENGTH WITH RADIAL POSITION

[Radial position r normalized to 1 at boundary r = a.]

Nondimensional radius, r/a	Root mean square magnitudes	Nondimensional radius to field penetration ratio, h										
		0.1	0.5	1.0	2.0	2.5	5.0	7.5	10	15	20	25
		$\alpha = 0$										
0	$\oint$	0.999	0.998	0.983	0.812	0.662	0.160	0.034	0.007	2×10^{-4}	8×10^{-6}	5×10^{-8}
	$\oint_1$	0	0	0	0	0	0	0	0	0	0	0
0.1	$\oint$	0.999	0.999	0.984	0.814	0.66	0.161	0.034	0.007	3×10^{-4}	1×10^{-5}	4×10^{-7}
	$\oint_1$	.100	.100	.100	.096	.091	.043	.013	.003	2×10^{-4}	9×10^{-6}	4×10^{-7}
0.2	$\oint$	0.999	0.999	0.984	0.814	0.662	0.163	0.036	0.008	5×10^{-4}	3×10^{-5}	2×10^{-6}
	$\oint_1$	.200	.200	.199	.192	.182	.086	.027	.007	4×10^{-4}	3×10^{-5}	2×10^{-6}
0.3	$\oint$	0.999	0.999	0.984	0.815	0.664	0.173	0.046	0.013	1×10^{-3}	9×10^{-5}	8×10^{-6}
	$\oint_1$	.300	.300	.299	.288	.273	.131	.042	.012	1×10^{-3}	9×10^{-5}	8×10^{-6}
0.4	$\oint$	0.999	0.999	0.984	0.819	0.672	0.197	0.066	0.023	3×10^{-3}	3×10^{-4}	4×10^{-5}
	$\oint_1$	.400	.400	.399	.385	.365	.179	.064	.022	3×10^{-3}	3×10^{-4}	4×10^{-5}
0.5	$\oint$	0.999	0.999	0.985	0.827	0.686	0.243	0.100	0.042	7×10^{-3}	0.001	2×10^{-4}
	$\oint_1$	.500	.500	.499	.482	.458	.236	.097	.040	7×10^{-3}	.001	2×10^{-4}
0.6	$\oint$	0.999	0.999	0.986	0.840	0.712	0.313	0.156	0.077	1.9×10^{-2}	0.005	1×10^{-3}
	$\oint_1$	.600	.600	.599	.579	.553	.310	.151	.075	1.8×10^{-2}	.004	1×10^{-3}
0.7	$\oint$	0.999	0.999	0.988	0.862	0.753	0.414	0.244	0.143	5×10^{-2}	0.017	4×10^{-3}
	$\oint_1$	.700	.700	.699	.679	.652	.419	.240	.142	4.9×10^{-2}	.017	6×10^{-3}
0.8	$\oint$	0.999	0.999	0.990	0.893	0.813	0.55	0.388	0.272	1.34×10^{-1}	0.066	3.3×10^{-2}
	$\oint_1$	.800	.800	.799	.782	.758	.546	.384	.270	1.33×10^{-1}	.066	3.2×10^{-2}
0.9	$\oint$	0.999	0.999	0.994	0.939	0.895	0.74	0.62	0.520	3.65×10^{-1}	0.256	1.8×10^{-1}
	$\oint_1$	.900	.900	.899	.888	.873	.736	.618	.518	3.64×10^{-1}	.260	1.8×10^{-1}
1.0	$\oint$	1.000	1.000	1.000	1.000	1.000	1.000	1.000	1.000	1.000	1.000	1.000
	$\oint_1$	1.000	1.000	1.000	1.000	1.000	1.000	1.000	1.000	1.000	1.000	1.000

TABLE II. - Continued. VARIATION OF ROOT MEAN SQUARE MAGNITUDES OF MAGNETIC-FLUX AND ELECTRIC-FIELD STRENGTH WITH RADIAL POSITION

[Radial position r normalized to 1 at boundary r = a.]

Nondimensional radius, r/a	Root mean square magnitudes	Nondimensional radius to field penetration ratio, h										
		0.1	0.5	1.0	2.0	2.5	5.0	7.5	10	15	20	25
		$\alpha = 1$										
0	$\mathcal{J}$	0.998	0.956	0.836	0.510	0.370	0.054	0.007	8×10^{-4}	9×10^{-6}	1×10^{-7}	1×10^{-9}
	$\mathcal{J}_1$	0	0	0	0	0	0	0	0	0	0	0
0.1	$\mathcal{J}$	0.998	0.957	0.840	0.517	0.375	0.056	0.007	9×10^{-4}	1×10^{-5}	2×10^{-7}	3×10^{-9}
	$\mathcal{J}_1$	.100	.098	.092	.071	.059	.015	.003	4×10^{-4}	9×10^{-6}	2×10^{-7}	3×10^{-9}
0.2	$\mathcal{J}$	0.998	0.958	0.845	0.528	0.387	0.064	0.010	0.001	4×10^{-5}	9×10^{-7}	2×10^{-8}
	$\mathcal{J}_1$	.200	.196	.184	.143	.119	.033	.006	.001	3×10^{-5}	8×10^{-7}	2×10^{-8}
0.3	$\mathcal{J}$	0.998	0.961	0.852	0.547	0.409	0.079	0.015	0.003	1×10^{-4}	4×10^{-6}	2×10^{-7}
	$\mathcal{J}_1$	.300	.294	.277	.218	.184	.054	.012	.003	1×10^{-4}	4×10^{-6}	2×10^{-7}
0.4	$\mathcal{J}$	0.999	0.964	0.863	0.575	0.442	0.105	0.025	0.006	4×10^{-4}	2×10^{-5}	2×10^{-6}
	$\mathcal{J}_1$	.400	.393	.371	.298	.255	.084	.023	.006	4×10^{-4}	2×10^{-5}	1×10^{-6}
0.5	$\mathcal{J}$	0.999	0.967	0.877	0.612	0.487	0.145	0.045	0.014	0.001	1×10^{-4}	1×10^{-5}
	$\mathcal{J}_1$	.500	.492	.468	.385	.334	.128	.042	.013	.001	1×10^{-4}	1×10^{-5}
0.6	$\mathcal{J}$	0.999	0.972	0.894	0.660	0.547	0.208	0.082	0.032	0.005	8×10^{-4}	1×10^{-4}
	$\mathcal{J}_1$	.600	.592	.567	.480	.426	.192	.078	.031	.005	8×10^{-4}	1×10^{-4}
0.7	$\mathcal{J}$	0.999	0.978	0.915	0.721	0.624	0.303	0.151	0.075	0.019	0.005	0.001
	$\mathcal{J}_1$	.700	.692	.669	.586	.534	.288	.146	.074	.019	.005	.001
0.8	$\mathcal{J}$	0.999	0.984	0.939	0.796	0.722	0.477	0.281	0.177	0.070	0.028	0.011
	$\mathcal{J}_1$	.800	.794	.775	.706	.661	.435	.276	.175	.070	.028	.011
0.9	$\mathcal{J}$	0.999	0.992	0.967	0.889	0.846	0.666	0.528	0.419	0.264	0.166	0.105
	$\mathcal{J}_1$	.900	.896	.885	.843	.815	.658	.524	.417	.263	.166	.104
1.0	$\mathcal{J}$	1.000	1.000	1.000	1.000	1.000	1.000	1.000	1.000	1.000	1.000	1.000
	$\mathcal{J}_1$	1.000	1.000	1.000	1.000	1.000	1.000	1.000	1.000	1.000	1.000	1.000

TABLE II. - Continued. VARIATION OF ROOT MEAN SQUARE MAGNITUDES OF MAGNETIC-FLUX AND ELECTRIC-FIELD STRENGTH WITH RADIAL POSITION

[Radial position r normalized to 1 at boundary r = a.]

Nondimensional radius, r/a	Root mean square magnitudes	Nondimensional radius to field penetration ratio, h										
		0.1	0.5	1.0	2.0	2.5	5.0	7.5	10	15	20	25
						$\alpha = 2$						
0	$\mathcal{J}$	0.998	0.945	0.807	0.466	0.326	0.042	0.005	5×10^{-4}	4×10^{-6}	4×10^{-8}	4×10^{-10}
	$\mathcal{J}_1$	0	0	0	0	0	0	0	0	0	0	0
0.1	$\mathcal{J}$	0.998	0.947	0.809	0.468	0.330	0.044	0.005	6×10^{-4}	7×10^{-6}	9×10^{-8}	1×10^{-9}
	$\mathcal{J}_1$	.099	.097	.090	.066	.053	.012	.002	3×10^{-4}	4×10^{-6}	6×10^{-8}	8×10^{-10}
0.2	$\mathcal{J}$	0.998	0.948	0.814	0.480	0.344	0.052	0.007	0.001	2×10^{-8}	4×10^{-7}	8×10^{-8}
	$\mathcal{J}_1$	.200	.195	.180	.133	.108	.026	.005	7×10^{-4}	2×10^{-5}	4×10^{-7}	7×10^{-9}
0.3	$\mathcal{J}$	0.998	0.951	0.823	0.502	0.368	0.067	0.012	0.002	7×10^{-5}	2×10^{-6}	7×10^{-8}
	$\mathcal{J}_1$	.300	.292	.271	.204	.168	.045	.009	.002	6×10^{-5}	2×10^{-6}	7×10^{-8}
0.4	$\mathcal{J}$	0.998	0.955	0.836	0.533	0.404	0.091	0.020	0.005	3×10^{-4}	1×10^{-5}	7×10^{-7}
	$\mathcal{J}_1$	.400	.391	.365	.281	.235	.072	.018	.004	2×10^{-4}	1×10^{-5}	7×10^{-7}
0.5	$\mathcal{J}$	0.998	0.959	0.853	0.574	0.452	0.129	0.038	0.011	0.001	8×10^{-5}	7×10^{-6}
	$\mathcal{J}_1$	.500	.490	.460	.365	.312	.111	.035	.010	9×10^{-4}	8×10^{-5}	7×10^{-6}
0.6	$\mathcal{J}$	0.999	0.965	0.873	0.628	0.516	0.189	0.071	0.027	0.004	5×10^{-4}	8×10^{-5}
	$\mathcal{J}_1$	.600	.589	.559	.460	.402	.172	.067	.026	.004	5×10^{-4}	8×10^{-5}
0.7	$\mathcal{J}$	0.999	0.972	0.898	0.695	0.598	0.282	0.135	0.065	0.015	0.003	8×10^{-4}
	$\mathcal{J}_1$	.700	.690	.662	.567	.511	.266	.131	.063	.015	.003	8×10^{-4}
0.8	$\mathcal{J}$	0.999	0.980	0.928	0.778	0.703	0.426	0.261	0.160	0.060	0.023	0.009
	$\mathcal{J}_1$	.800	.792	.769	.690	.642	.413	.256	.158	.060	.022	.009
0.9	$\mathcal{J}$	0.999	0.990	0.961	0.878	0.835	0.650	0.509	0.399	0.245	0.151	0.093
	$\mathcal{J}_1$	.900	.895	.882	.833	.803	.641	.505	.397	.244	.150	.092
1.0	$\mathcal{J}$	1.000	1.000	1.000	1.000	1.000	1.000	1.000	1.000	1.000	1.000	1.000
	$\mathcal{J}_1$	1.000	1.000	1.000	1.000	1.000	1.000	1.000	1.000	1.000	1.000	1.000

TABLE II. - Concluded. VARIATION OF ROOT MEAN SQUARE MAGNITUDES OF MAGNETIC-FLUX AND ELECTRIC-FIELD STRENGTH WITH RADIAL POSITION

[Radial position r normalized to 1 at boundary r = a.]

Nondimensional radius, r/a	Root mean square magnitudes	Nondimensional radius to field penetration ratio, h										
		0.1	0.5	1.0	2.0	2.5	5.0	7.5	10	15	20	25
		$\alpha = >> 1$										
0	$\mathcal{J}$	0.998	0.940	0.789	0.439	0.304	0.037	0.004	4×10^{-4}	3×10^{-6}	2×10^{-8}	2×10^{-10}
	$\mathcal{J}_1$	0	0	0	0	0	0	0	0	0	0	0
0.1	$\mathcal{J}$	0.998	0.941	0.791	0.443	0.309	0.039	0.004	5×10^{-4}	5×10^{-6}	5×10^{-8}	6×10^{-10}
	$\mathcal{J}_1$	.100	.097	.089	.063	.050	.011	.002	2×10^{-4}	3×10^{-6}	4×10^{-8}	4×10^{-10}
0.2	$\mathcal{J}$	0.998	0.943	0.797	0.456	0.323	0.046	0.006	8×10^{-4}	1×10^{-5}	3×10^{-7}	5×10^{-5}
	$\mathcal{J}_1$	.200	.194	.178	.128	.102	.023	.004	6×10^{-4}	1×10^{-5}	2×10^{-7}	4×10^{-9}
0.3	$\mathcal{J}$	0.998	0.946	0.807	0.479	0.348	0.060	0.010	0.002	5×10^{-5}	2×10^{-6}	5×10^{-6}
	$\mathcal{J}_1$	.300	.292	.268	.197	.160	.040	.008	.001	5×10^{-5}	1×10^{-6}	4×10^{-8}
0.4	$\mathcal{J}$	0.998	0.950	0.821	0.512	0.384	0.083	0.018	0.004	2×10^{-4}	1×10^{-5}	5×10^{-7}
	$\mathcal{J}_1$	.400	.390	.361	.272	.225	.065	.016	.004	2×10^{-4}	9×10^{-6}	5×10^{-7}
0.5	$\mathcal{J}$	0.998	0.955	0.839	0.555	0.435	0.121	0.034	0.010	8×10^{-4}	7×10^{-5}	5×10^{-6}
	$\mathcal{J}_1$	.500	.488	.456	.355	.300	.103	.031	.009	8×10^{-4}	6×10^{-5}	5×10^{-6}
0.6	$\mathcal{J}$	0.999	0.962	0.862	0.611	0.501	0.179	0.065	0.024	0.003	4×10^{-4}	6×10^{-5}
	$\mathcal{J}_1$	.600	.588	.555	.449	.390	.162	.062	.023	.003	4×10^{-4}	6×10^{-5}
0.7	$\mathcal{J}$	0.999	0.969	0.888	0.681	0.585	0.271	0.127	0.060	0.013	0.003	7×10^{-4}
	$\mathcal{J}_1$	.700	.689	.658	.557	.499	.255	.123	.058	.013	.003	7×10^{-4}
0.8	$\mathcal{J}$	0.999	0.978	0.920	0.768	0.693	0.415	0.251	0.152	0.056	0.021	0.008
	$\mathcal{J}_1$	.800	.791	.766	.682	.632	.401	.246	.150	.055	.020	.008
0.9	$\mathcal{J}$	0.999	0.989	0.957	0.873	0.829	0.642	0.499	0.388	0.235	0.143	0.086
	$\mathcal{J}_1$	.900	.895	.880	.828	.796	.632	.495	.386	.235	.142	.086
1.0	$\mathcal{J}$	1.000	1.000	1.000	1.000	1.000	1.000	1.000	1.000	1.000	1.000	1.000
	$\mathcal{J}_1$	1.000	1.000	1.000	1.000	1.000	1.000	1.000	1.000	1.000	1.000	1.000

TABLE III. - VARIATION OF PHASE ANGLES BETWEEN FIELDS IN PLASMA AND THOSE AT BOUNDARY (r = a)[a]

Nondimensional radius, r/a	Phase angle	Nondimensional radius to field penetration ratio, h										
		0.1	0.5	1.0	2.0	2.5	5.0	7.5	10	15	20	25
		$\alpha = 0$										
0	φ	0.145	3.6	14.3	52.3	74.7	178.9	280.6	382.1	564.9	787.5	990.2
	φ_1	.072	1.8	7.2	28.3	43.4	138.6	238.6	331.3	556.5	743.6	946.0
0.1	φ	0.142	3.5	14.1	51.7	73.8	175.4	272.6	367.9	526.3	735.2	915.5
	φ_1	.071	1.8	7.1	28	42.9	136.8	234.6	332.1	525.2	715.3	902.6
0.2	φ	0.138	3.4	13.7	50	71.1	164.7	249.5	329.8	468.3	649.3	811.2
	φ_1	.069	1.7	6.9	27.1	41.6	131.4	222.6	311.0	480.3	644.7	807.4
0.3	φ	0.130	3.3	12.9	47.1	66.6	147.7	210.0	285.6	426.3	567.9	709.5
	φ_1	.065	1.6	6.5	25.7	39.4	122.5	203.1	278.6	422.6	565.1	707.4
0.4	φ	0.120	3.0	11.9	43.2	60.4	126.6	184.0	243.9	365.2	486.6	608.1
	φ_1	.060	1.5	6.0	23.7	36.2	110.3	177.9	240.4	362.8	484.9	606.7
0.5	φ	0.107	2.7	10.7	38.1	52.6	104.3	152.3	203.1	304.2	405.4	506.6
	φ_1	.054	1.3	5.4	21.1	32.2	95.2	149.4	200.7	302.7	404.3	505.8
0.6	φ	0.092	2.3	9.1	32.0	43.5	82.4	122.0	162.5	223.3	324.3	405.3
	φ_1	.046	1.2	4.4	18.0	27.3	77.8	119.9	160.8	242.3	323.6	404.7
0.7	φ	0.073	1.4	7.2	24.9	33.2	61.3	91.5	121.8	182.5	243.3	303.9
	φ_1	.037	.9	3.5	14.3	21.6	59.1	90.1	120.8	181.8	242.7	303.6
0.8	φ	0.052	1.3	5.1	17.1	22.4	40.7	60.9	81.2	121.6	162.1	202.6
	φ_1	.026	.7	2.4	10.0	15.1	39.6	60.1	80.6	121.2	161.9	202.5
0.9	φ	0.027	0.7	2.7	8.8	11.2	20.3	30.5	40.6	60.8	81.1	101.3
	φ_1	.014	.4	1.4	5.3	7.9	19.9	30.1	40.3	60.6	80.9	101.2
1.0	φ	0	0	0	0	0	0	0	0	0	0	0
	φ_1	0	0	0	0	0	0	0	0	0	0	0

[a]Fields in the plasma always lag behind those at r = a, and the absolute values of the phase angles in degrees are presented herein.

TABLE III. - Continued. VARIATION OF PHASE ANGLES BETWEEN FIELDS IN PLASMA AND THOSE AT BOUNDARY (r = a)[a]

Nondimensional radius, r/a	Phase angle	Nondimensional radius to field penetration ratio, h										
		0.1	0.5	1.0	2.0	2.5	5.0	7.5	10	15	20	25
$\alpha = 1$												
0	φ	0.102	2.50	9.30	30.5	41.6	97.7	152.8	207.7	317.5	427.1	530.0
	φ_1	.051	1.26	4.99	18.3	27.0	78.8	135.2	187.5	290.0	419.0	520.0
0.1	φ	0.100	2.45	9.20	29.7	40.9	95.2	147.3	198.4	298.4	397.1	495.2
	φ_1	.050	1.24	4.89	17.9	26.5	76.7	129.2	181.5	275.0	387.1	487.9
0.2	φ	0.097	2.38	8.90	28.5	39.1	88.4	133.8	177.6	254.5	351.6	439.1
	φ_1	.049	1.21	4.72	17.3	25.6	73.0	121.3	168.3	259.4	348.5	436.8
0.3	φ	0.092	2.25	8.40	26.6	36.1	78.7	117.0	154.7	230.9	307.4	384.0
	φ_1	.046	1.14	4.46	16.3	24.0	67.2	109.6	150.1	228.5	307.8	382.8
0.4	φ	0.085	2.07	7.70	24.0	32.2	67.6	99.8	132.2	197.7	263.4	329.1
	φ_1	.043	1.05	4.11	15.0	21.9	59.8	95.6	129.7	196.3	262.4	328.3
0.5	φ	0.076	1.85	6.83	20.8	27.7	56.1	82.9	110.0	164.7	219.5	274.2
	φ_1	.038	.94	3.66	13.2	19.3	51.1	80.4	108.5	163.8	218.8	273.7
0.6	φ	0.065	1.57	5.77	17.2	22.5	44.7	66.2	88.0	131.7	175.5	219.3
	φ_1	.032	.80	3.12	11.1	16.1	41.6	64.7	87.0	131.1	175.1	219.1
0.7	φ	0.052	1.25	4.55	13.2	17.1	33.4	49.6	65.9	98.8	131.6	164.5
	φ_1	.026	.64	2.47	8.8	12.6	31.6	48.7	65.3	98.4	131.4	164.3
0.8	φ	0.036	0.88	3.17	8.9	11.5	22.2	33.0	43.9	65.8	87.7	109.7
	φ_1	.018	.45	1.74	6.1	8.7	21.2	32.5	43.6	65.6	87.6	109.5
0.9	φ	0.019	0.46	1.65	4.5	5.7	11.1	16.5	22.0	32.9	43.9	54.8
	φ_1	.010	.24	.91	3.2	4.5	10.7	16.3	21.8	32.8	43.8	54.8
1.0	φ	0	0	0	0	0	0	0	0	0	0	0
	φ_1	0	0	0	0	0	0	0	0	0	0	0

[a]Fields in the plasma always lag behind those at r = a, and the absolute values of the phase angles in degrees are presented herein.

TABLE III. - Continued. VARIATION OF PHASE ANGLES BETWEEN FIELDS IN PLASMA AND THOSE AT BOUNDARY (r = a)[a]

Nondimensional radius, r/a	Phase angle	Nondimensional radius to field penetration ratio, h										
		0.1	0.5	1.0	2.0	2.5	5.0	7.5	10	15	20	25
		$\alpha = 2$										
0	φ	0.064	1.560	5.81	18.30	25.1	58.7	91.8	124.8	190.7	256.5	320.0
	φ_1	.064	.790	3.10	11.40	16.9	47.8	82.0	112.0	182.0	260.0	319.0
0.1	φ	0.063	1.540	5.71	18.00	24.7	57.2	88.4	119.0	179.0	238.3	297.3
	φ_1	.032	.785	3.06	11.10	16.3	46.4	77.8	109.2	171.2	232.4	292.9
0.2	φ	0.061	1.490	5.52	17.30	23.5	53.0	80.2	106.5	158.8	211.1	263.6
	φ_1	.031	.761	2.96	10.70	15.7	44.1	72.9	101.0	155.7	209.2	262.3
0.3	φ	0.058	1.410	5.21	16.00	21.7	47.1	70.2	92.9	138.6	184.6	230.6
	φ_1	.029	.721	2.80	10.10	14.7	40.5	65.8	90.0	137.1	183.6	229.9
0.4	φ	0.054	1.300	4.77	14.40	19.3	40.5	59.9	79.4	118.7	158.1	197.6
	φ_1	.027	.665	2.58	9.23	13.4	35.9	57.3	77.8	117.8	157.5	197.1
0.5	φ	0.048	1.160	4.22	12.50	16.5	33.7	49.8	66.1	98.9	131.7	164.6
	φ_1	.024	.594	2.30	8.14	11.8	30.7	48.2	65.1	98.3	131.3	164.3
0.6	φ	0.041	0.987	3.56	10.30	13.4	26.8	39.7	52.8	79.1	105.3	131.7
	φ_1	.020	.506	1.95	6.85	9.8	24.9	38.8	52.2	78.7	105.1	131.5
0.7	φ	0.033	0.784	2.80	7.87	10.2	20.0	29.8	39.6	59.3	79.0	98.8
	φ_1	.016	.403	1.55	5.37	7.6	18.9	29.2	39.2	59.1	78.9	98.6
0.8	φ	0.023	0.551	1.95	5.33	6.8	13.3	19.8	26.4	39.5	52.7	65.8
	φ_1	.012	.284	1.09	3.72	5.3	12.7	19.5	26.2	39.4	52.6	65.8
0.9	φ	0.012	0.290	1.01	2.69	3.4	6.7	9.9	13.2	19.8	26.3	32.9
	φ_1	.006	.150	.57	1.92	2.7	6.4	9.8	13.1	19.7	26.3	32.9
1.0	φ	0	0	0	0	0	0	0	0	0	0	0
	φ_1	0	0	0	0	0	0	0	0	0	0	0

[a]Fields in the plasma always lag behind those at r = a, and the absolute values of the phase angles in degrees are presented herein.

TABLE III. - Continued. VARIATION OF PHASE ANGLES BETWEEN FIELDS IN PLASMA AND THOSE AT BOUNDARY (r = a)[a]

Nondimensional radius, r/a	Phase angle	Nondimensional radius to field penetration ratio, h										
		0.1	0.5	1.0	2.0	2.5	5.0	7.5	10	15	20	25
$\alpha = 3$												
0	φ	0.047	1.120	4.08	12.90	17.5	41.0	64.0	87.0	133.0	178.9	228.1
	φ_1	.022	.564	2.20	7.90	11.6	33.2	56.7	79.6	121.5	170.0	221.0
0.1	φ	0.045	1.090	4.02	12.60	17.2	39.9	61.7	83.0	124.8	166.1	207.3
	φ_1	.022	.555	2.16	7.80	11.4	32.4	54.3	76.2	119.4	162.0	206.2
0.2	φ	0.043	1.050	3.88	12.10	16.4	36.9	55.9	74.3	110.7	147.2	183.8
	φ_1	.022	.538	2.09	7.53	11.0	30.8	50.8	70.4	108.5	145.8	182.8
0.3	φ	0.041	0.998	3.66	11.20	15.1	32.8	48.9	64.8	96.6	128.7	160.7
	φ_1	.021	.510	1.98	7.09	10.3	28.3	45.9	62.8	95.6	128.0	160.2
0.4	φ	0.038	0.920	3.35	10.10	13.5	28.2	41.8	55.3	82.8	110.2	137.7
	φ_1	.019	.470	1.82	6.48	9.4	25.1	40.0	54.2	82.1	109.8	137.4
0.5	φ	0.034	0.820	2.96	8.71	11.5	23.4	34.7	46.1	68.9	91.8	114.8
	φ_1	.017	.420	1.62	5.71	8.2	21.4	33.6	45.4	68.5	91.6	114.6
0.6	φ	0.029	0.700	2.50	7.16	9.4	18.7	27.7	36.8	55.1	73.5	91.8
	φ_1	.014	.358	1.38	4.80	6.9	17.4	27.0	36.4	54.9	73.3	91.7
0.7	φ	0.023	0.553	1.96	5.48	7.1	14.0	20.8	27.6	41.3	55.1	68.9
	φ_1	.012	.285	1.09	3.76	5.3	13.2	20.4	27.3	41.2	55.0	68.8
0.8	φ	0.016	0.389	1.37	3.71	4.8	9.3	13.8	18.4	27.6	36.7	45.9
	φ_1	.008	.201	.77	2.61	3.7	8.9	13.6	18.2	27.5	36.7	45.6
0.9	φ	0.009	0.204	0.71	1.87	2.4	4.6	6.9	9.2	13.8	18.4	22.9
	φ_1	.004	.106	.40	1.35	1.9	4.5	6.8	9.1	13.7	18.3	22.9
1.0	φ	0	0	0	0	0	0	0	0	0	0	0
	φ_1	0	0	0	0	0	0	0	0	0	0	0

[a]Fields in the plasma always lag behind those at r = a, and the absolute values of the phase angles in degrees are presented herein.

TABLE III. - Continued. VARIATION OF PHASE ANGLES BETWEEN FIELDS IN PLASMA AND THOSE AT BOUNDARY (r = a)[a]

Nondimensional radius, r/a	Phase angle	Nondimensional radius to field penetration ratio, h										
		0.1	0.5	1.0	2.0	2.5	5.0	7.5	10	15	20	25
		$\alpha = 5$										
0	φ	0.029	0.685	2.52	7.87	10.80	25.2	39.4	53.4	81.8	110.1	138.0
	φ_1	.014	.352	1.37	4.91	7.17	20.5	35.4	49.6	78.3	109.7	136.0
0.1	φ	0.028	0.675	2.48	7.76	10.62	24.5	37.9	51.0	76.8	102.2	127.5
	φ_1	.014	.344	1.34	4.82	7.06	19.9	33.4	46.9	73.5	99.7	125.6
0.2	φ	0.027	0.654	2.40	7.43	10.10	22.7	34.4	45.7	68.1	90.6	113.1
	φ_1	.014	.334	1.29	4.65	6.80	18.9	31.3	43.3	66.8	89.7	112.5
0.3	φ	0.026	0.619	2.26	6.90	9.39	20.2	30.1	39.8	59.5	79.1	98.9
	φ_1	.013	.316	1.22	4.38	6.37	17.4	28.2	38.6	58.8	78.7	98.6
0.4	φ	0.024	0.570	2.07	6.20	8.28	17.3	25.7	34.1	50.9	67.8	84.7
	φ_1	.012	.292	1.13	4.00	5.79	15.4	24.6	33.4	50.5	67.6	84.5
0.5	φ	0.021	0.507	1.83	5.36	7.07	14.4	21.3	28.3	42.4	56.5	70.6
	φ_1	.011	.260	1.00	3.53	5.08	13.1	20.7	27.9	42.2	56.3	70.5
0.6	φ	0.018	0.432	1.54	4.40	5.75	11.5	17.0	22.7	33.9	45.2	56.5
	φ_1	.009	.222	.85	2.96	4.24	10.7	16.6	22.4	33.8	45.1	56.4
0.7	φ	0.014	0.343	1.21	3.37	4.36	8.6	12.8	17.0	25.4	33.9	42.4
	φ_1	.007	.176	.68	2.32	3.30	8.1	12.5	16.8	25.3	33.8	42.3
0.8	φ	0.010	0.241	0.84	2.28	2.92	5.7	8.5	11.3	17.0	22.6	28.2
	φ_1	.005	.124	.47	1.61	2.27	5.5	8.4	11.2	16.9	22.6	28.2
0.9	φ	0.005	0.126	0.44	1.15	1.46	2.9	4.3	5.7	8.5	11.3	14.1
	φ_1	.003	.066	.25	.83	1.16	2.7	4.2	5.6	8.5	11.3	24.1
1.0	φ	0	0	0	0	0	0	0	0	0	0	0
	φ_1	0	0	0	0	0	0	0	0	0	0	0

[a] Fields in the plasma always lag behind those at r = a, and the absolute values of the phase angles in degrees are presented herein.

TABLE III. - Continued. VARIATION OF PHASE ANGLES BETWEEN FIELDS IN PLASMA AND THOSE AT BOUNDARY (r = a)[a]

Nondimensional radius, r/a	Phase angle	Nondimensional radius to field penetration ratio, h										
		0.1	0.5	1.0	2.0	2.5	5.0	7.5	10	15	20	25
α = 10												
0	φ	0.014	0.349	1.280	4.02	5.46	12.70	19.90	27.10	41.4	55.6	71.8
	φ_1	.007	.178	.681	2.49	3.65	10.40	17.50	24.50	38.7	54.3	70.0
0.1	φ	0.014	0.342	1.260	3.93	5.37	12.40	19.20	25.80	38.8	51.7	64.5
	φ_1	.007	.175	.678	2.44	3.57	10.10	16.90	23.70	37.1	50.4	63.5
0.2	φ	0.014	0.331	1.220	3.76	5.11	11.50	17.40	23.10	34.4	45.8	57.2
	φ_1	.007	.169	.656	2.36	3.44	9.58	15.80	21.90	33.7	45.3	56.9
0.3	φ	0.013	0.314	1.150	3.49	4.71	10.20	15.20	20.10	30.1	40.0	49.9
	φ_1	.007	.160	.621	2.22	3.23	8.79	14.30	19.50	29.7	39.8	49.8
0.4	φ	0.012	0.289	1.050	3.14	4.18	8.76	13.00	17.20	25.7	34.3	42.8
	φ_1	.006	.148	.572	2.03	2.93	7.79	12.40	16.90	25.5	34.2	42.7
0.5	φ	0.011	0.257	0.927	2.71	3.58	7.30	10.80	14.30	21.4	28.6	35.7
	φ_1	.005	.132	.508	1.79	2.57	6.65	10.50	14.10	21.3	28.5	35.6
0.6	φ	0.009	0.219	0.782	2.23	2.91	5.81	8.62	11.50	17.1	22.8	28.6
	φ_1	.005	.112	.432	1.50	2.14	5.40	8.41	11.30	17.1	22.8	28.5
0.7	φ	0.007	0.174	0.614	1.70	2.20	4.35	6.45	8.58	12.9	17.1	21.4
	φ_1	.004	.089	.343	1.18	1.67	4.10	6.33	8.50	12.8	17.1	21.4
0.8	φ	0.005	0.122	0.427	1.15	1.48	2.89	4.30	5.72	8.6	11.4	14.3
	φ_1	.003	.063	.240	.81	1.15	2.75	4.23	5.67	8.5	11.4	14.3
0.9	φ	0.003	0.064	0.221	0.58	0.74	1.44	2.15	2.86	4.3	5.7	7.1
	φ_1	.001	.033	.126	.42	.59	1.38	2.12	2.84	4.3	5.7	7.1
1.0	φ	0	0	0	0	0	0	0	0	0	0	0
	φ_1	0	0	0	0	0	0	0	0	0	0	0

[a]Fields in the plasma always lag behind those at r = a, and the absolute values of the phase angles in degrees are presented herein.

TABLE III. - Continued. VARIATION OF PHASE ANGLES BETWEEN FIELDS IN PLASMA AND THOSE AT BOUNDARY (r = a)[a]

Nondimensional radius, r/a	Phase angle	Nondimensional radius to field penetration ratio, h										
		0.1	0.5	1.0	2.0	2.5	5.0	7.5	10	15	20	25
		α = 25										
0	φ	0.006	0.139	0.512	1.620	2.19	5.11	7.99	10.90	16.60	22.30	29.30
	φ_1	.003	.071	.280	.995	1.46	4.15	6.93	10.10	15.90	21.30	28.30
0.1	φ	0.006	0.137	0.505	1.580	2.15	4.98	7.69	10.40	15.60	20.70	25.90
	φ_1	.003	.070	.270	.980	1.43	4.05	6.78	9.51	14.90	20.20	25.50
0.2	φ	0.006	0.133	0.490	1.510	2.05	4.60	6.97	9.27	13.80	18.40	22.90
	φ_1	.003	.068	.260	.950	1.38	3.84	6.35	8.79	13.50	18.20	22.80
0.3	φ	0.005	0.126	0.460	1.400	1.89	4.09	6.10	8.08	12.10	16.10	20.30
	φ_1	.002	.064	.250	.890	1.29	3.53	5.72	7.83	11.90	16.00	20.00
0.4	φ	0.005	0.116	0.420	1.260	1.68	3.52	5.21	6.91	10.30	13.80	17.20
	φ_1	.002	.059	.230	.810	1.18	3.13	4.99	6.77	10.30	13.70	17.10
0.5	φ	0.004	0.103	0.370	1.090	1.43	2.93	4.33	5.75	8.60	11.50	14.30
	φ_1	.002	.053	.200	.720	1.03	2.67	4.19	5.66	8.55	11.40	14.30
0.6	φ	0.004	0.088	0.310	0.890	1.17	2.33	3.46	4.59	6.88	9.18	11.50
	φ_1	.002	.045	.170	.600	.86	2.17	3.37	4.54	6.85	9.15	11.40
0.7	φ	0.003	0.070	0.250	0.680	0.88	1.74	2.59	3.44	5.16	6.87	8.59
	φ_1	.002	.036	.140	.470	.67	1.64	2.54	3.41	5.14	6.86	8.58
0.8	φ	0.002	0.049	0.170	0.460	0.59	1.16	1.73	2.30	3.44	4.58	5.73
	φ_1	.001	.025	.100	.330	.46	1.10	1.70	2.28	3.43	4.57	5.72
0.9	φ	0.001	0.026	0.089	0.230	0.30	0.58	0.86	1.15	1.72	2.29	2.86
	φ_1	.001	.013	.050	.170	.24	.56	.85	1.14	1.71	2.29	2.86
1.0	φ	0	0	0	0	0	0	0	0	0	0	0
	φ_1	0	0	0	0	0	0	0	0	0	0	0

[a]Fields in the plasma always lag behind those at r = a, and the absolute values of the phase angles in degrees are presented herein.

TABLE III. - Concluded. VARIATION OF PHASE ANGLES BETWEEN FIELDS IN PLASMA AND THOSE AT BOUNDARY (r = a)[a]

Nondimensional radius, r/a	Phase angle	Nondimensional radius to field penetration ratio, h									
		0.1	0.5	1.0	2.0	2.5	5.0	7.5	10	15	20	25
α = 100												
0	φ	0.0010	0.035	0.128	0.401	0.548	1.28	1.99	2.72	4.15	5.58	7.19
	φ_1	.0007	.019	.069	.250	.370	1.04	1.78	2.40	4.00	5.50	7.06
0.1	φ	0.0010	0.034	0.126	0.394	0.539	1.24	1.92	2.59	3.90	5.18	6.47
	φ_1	.0007	.018	.068	.245	.360	1.01	1.70	2.38	3.73	5.06	6.37
0.2	φ	0.0010	0.033	0.122	0.377	0.513	1.15	1.74	2.32	3.46	4.59	5.74
	φ_1	.0007	.017	.066	.237	.350	.96	1.59	2.20	3.39	4.55	5.71
0.3	φ	0.0010	0.032	0.115	0.350	0.472	1.02	1.51	2.02	3.02	4.02	5.02
	φ_1	.0007	.016	.062	.223	.320	.88	1.43	1.96	2.98	3.99	5.00
0.4	φ	0.0010	0.029	0.105	0.314	0.420	0.88	1.30	1.73	2.58	3.44	4.30
	φ_1	.0006	.015	.057	.203	.290	.78	1.25	1.69	2.56	3.43	4.29
0.5	φ	0.0010	0.026	0.093	0.272	0.359	0.73	1.08	1.44	2.15	2.87	3.58
	φ_1	.0005	.013	.051	.179	.260	.67	1.05	1.42	2.14	2.86	3.58
0.6	φ	0.0010	0.022	0.079	0.220	0.292	0.58	0.86	1.15	1.72	2.29	2.87
	φ_1	.0005	.011	.043	.151	.210	.54	.84	1.14	1.71	2.29	2.86
0.7	φ	0.0010	0.017	0.062	0.170	0.221	0.44	0.65	0.86	1.29	1.72	2.15
	φ_1	.0004	.009	.034	.118	.170	.41	.64	.85	1.29	1.72	2.15
0.8	φ	0.0010	0.012	0.043	0.120	0.148	0.29	0.43	0.57	0.86	1.15	1.43
	φ_1	.0003	.006	.024	.082	.120	.28	.42	.57	.86	1.14	1.43
0.9	φ	0.0003	0.006	0.022	0.060	0.074	0.14	0.22	0.29	0.43	0.57	0.72
	φ_1	.0004	.003	.013	.042	.060	.14	.21	.28	.43	.57	.72
1.0	φ	0	0	0	0	0	0	0	0	0	0	0
	φ_1	0	0	0	0	0	0	0	0	0	0	0

[a] Fields in the plasma always lag behind those at r = a, and the absolute values of the phase angles in degrees are presented herein.

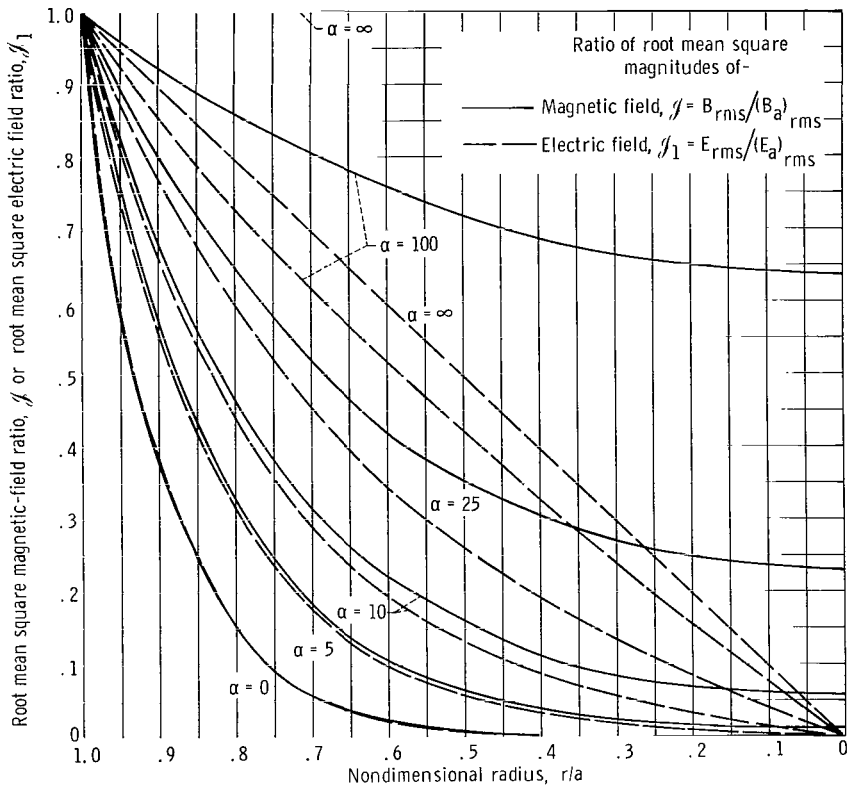

Figure 10. - Radial penetrations of the magnetic and electric fields with α as parameter for radius to skin depth ratio of 10.

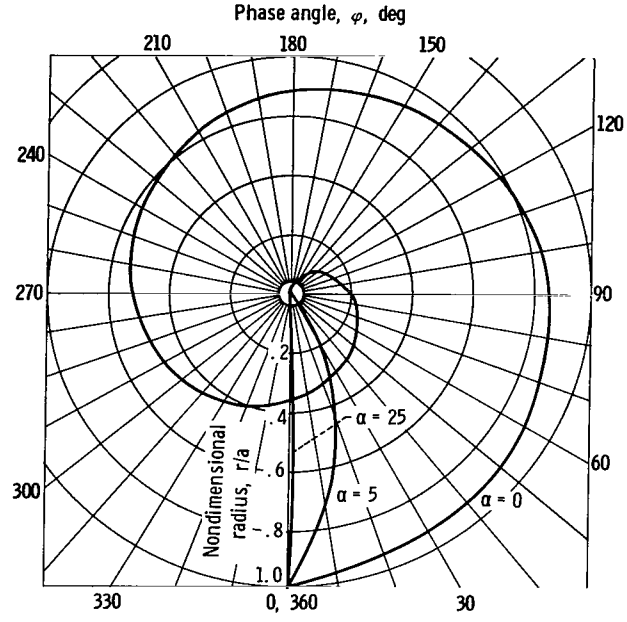

(a) Magnetic field.

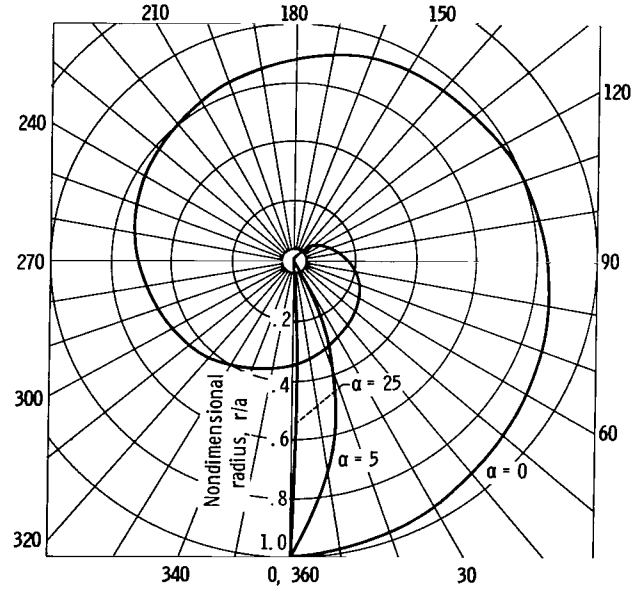

(b) Electric field.

Figure 11. - Radial variation of phase differences between fields in the plasma and that those at boundary (r = a).

APPENDIX C

SOLUTIONS WHEN $\alpha \gg 1$

Solutions for Nondimensional Power

Using equations (30) and (31), the nondimensional power given by equation (34) may be rewritten as

$$\tilde{P} = \frac{\delta}{4a} \frac{\left(1 + \alpha^2\right)^{1/4}}{\sin\left(\frac{\cot^{-1}\alpha}{2}\right)} \operatorname{Re}\left[\frac{J_1(\xi_a)}{J_0(\xi_a)} \exp\left(\frac{-i \cot^{-1}\alpha}{2}\right)\right] \tag{C1}$$

When $\alpha \gg 1$, the following relations hold

$$\exp\left(\frac{-i \cot^{-1}\alpha}{2}\right) \longrightarrow \exp\left(\frac{-i}{2\alpha}\right) \tag{C2}$$

$$\sin\left(\frac{\cot^{-1}\alpha}{2}\right) \longrightarrow \frac{1}{2\alpha} \tag{C3}$$

$$\xi_a = \frac{\sqrt{2}\, a}{\delta \sqrt{\alpha}} i \exp\left(\frac{i}{2\alpha}\right) \longrightarrow hi \exp\left(\frac{i}{2\alpha}\right) \tag{C4}$$

Substituting these values into equation (C1) yields

$$\tilde{P} = \frac{\alpha}{\sqrt{2}\, h} \operatorname{Re}\left\{\frac{J_1\left[hi \exp\left(\frac{i}{2\alpha}\right)\right]}{J_0\left[hi \exp\left(\frac{i}{2\alpha}\right)\right]} \exp\left(-\frac{i}{2\alpha}\right)\right\} \tag{C5}$$

Using the series definition of the Bessel functions yields, when $\alpha \gg 1$,

$$J_0\left[hi \exp\left(\frac{i}{2\alpha}\right)\right] \cong I_0(h) + \frac{hi}{2\alpha} I_1(h) \tag{C6}$$

and

$$J_1\left[hi \exp\left(\frac{i}{2\alpha}\right)\right] \cong \exp\left(\frac{i}{2\alpha}\right)\left[iI_1(h) - \frac{h}{2\alpha} I_2(h)\right] \tag{C7}$$

Equation (C5) becomes, therefore

$$\tilde{P} = \frac{\alpha}{\sqrt{2}\ h}\ \mathrm{Re}\left\{\frac{\exp\left(\frac{i}{2\alpha}\right)\left[iI_1(h) - \frac{h}{2\alpha}\ I_2(h)\right]}{I_0(h) + \frac{hi}{2\alpha}\ I_1(h)}\ \exp\left(-\frac{i}{2\alpha}\right)\right\} \tag{C8}$$

where the I(h)'s are the modified Bessel functions. Reducing equation (C8) and rationalizing yield

$$\tilde{P} = \frac{1}{2\sqrt{2}}\left[\frac{I_1^2(h) - I_0(h)I_2(h)}{I_0^2(h) + \frac{h^2}{4\alpha^2}\ I^2(h)}\right] \tag{C9}$$

For $\alpha >> 1$, the second term in the denominator will be very small compared with $I_0^2(h)$ and equation (C9) reduces to

$$\tilde{P} = \frac{1}{2\sqrt{2}}\left[\frac{I_1^2(h)}{I_0^2(h)} - \frac{I_2(h)}{I_0(h)}\right] \tag{38}$$

Solution for Change in Inductance

The solution for $\Delta L/L_{op}$ is given by equations (45) and (42) as

$$\frac{\Delta L}{L_{op}} = 1 - \frac{\delta}{a}\left\{\left[\left(1 + \alpha^2\right)^{1/2} + \alpha\right]^{1/2} \mathrm{Im}\left[\frac{J_1(\xi_a)}{J_0(\xi_a)}\right] - \left[\left(1 + \alpha^2\right)^{1/2} - \alpha\right]^{1/2} \mathrm{Re}\left[\frac{J_1(\xi_a)}{J_0(\xi_a)}\right]\right\} \tag{C11}$$

Using equations (35) and (18) and simplifying yield

$$\frac{\Delta L}{L_{op}} = 1 - \frac{\sqrt{2}}{h}\left\{\sqrt{2}\ \cos\left(\frac{\cot^{-1}\alpha}{2}\right)\mathrm{Im}\left[\frac{J_1(\xi_a)}{J_0(\xi_a)}\right] - \sqrt{2}\ \sin\left(\frac{\cot^{-1}\alpha}{2}\right)\mathrm{Re}\left[\frac{J_1(\xi_a)}{J_0(\xi_a)}\right]\right\} \tag{C12}$$

or

$$\frac{\Delta L}{L_{op}} = 1 - \frac{2}{h} \operatorname{Im}\left[\frac{J_1(\xi_a)}{J_0(\xi_a)} \exp\left(-\frac{i}{2} \cot^{-1}\alpha\right)\right] \tag{C13}$$

For $\alpha >> 1$, using equations (C2) and (C4) yields

$$\frac{\Delta L}{L_{op}} = 1 - \frac{2}{h} \operatorname{Im} \frac{J_1\left[hi \exp\left(\frac{i}{2\alpha}\right)\right]}{J_0\left[hi \exp\left(\frac{i}{2\alpha}\right)\right]} \exp\left(-\frac{i}{2\alpha}\right) \tag{C14}$$

Using equations (C6) and (C7) and rationalizing yields

$$\frac{\Delta L}{L_{op}} = 1 - \frac{2}{h} \frac{I_0(h)I_1(h) + \frac{h^2}{4\alpha^2} I_1(h)I_2(h)}{I_0^2(h) + \frac{h^2}{4\alpha^2} I_1^2(h)} \tag{C15}$$

or for $\alpha >> 1$

$$\Delta L = L_{op}\left[1 - \frac{2}{h} \frac{I_1(h)}{I_0(h)}\right] \tag{46}$$

APPENDIX D

DETERMINATION OF CIRCUIT PARAMETERS AND CIRCUIT CHECK

The measurement of the coil current and inductance was complicated by the fact that the operating frequency of the system is near the self-resonant frequency of the coil when the stray capacitance of the Faraday shield is taken into consideration. In order to determine whether or not a true measurement of the coil current and inductance was obtained, it was necessary to determine the values of the individual circuit parameters. With this knowledge a check may be made of the validity of the various current and voltage measurements by checking the system when no plasma is present. The circuit parameters that must be determined are the coil inductance L_0, the lead inductance from the coil to ground, the inductance of the strap connecting the variable capacitors plus the lead to the coil inductance L_2, and the stray capacitance C_s (fig. 5, p. 16).

The inductance of the coil was calculated by using the equation (Welsby, ref. 13)

$$L_0 = \frac{4\pi^2 N^2 b^2}{l} K_n C_c \times 10^{-9} \text{ microhenries} \tag{D1}$$

where K_n is a correction factor used for short coils

$$K_n = \frac{1}{1 + 0.9\left(\frac{b}{l}\right) - 0.02\left(\frac{b}{l}\right)^2} \tag{D2}$$

and C_c is a correction factor used for the spacing of the coil turns

$$C_c = \left[1 - \frac{l(A' + B')}{\pi b N K_n}\right] \tag{D3}$$

where $A' = 2.3 \log_{10} d'/c$, $B' = 0.366\left[1 - 2.5/N + 3.8/N^2\right]$, d' is the diameter of the coil tubing, and c is the winding pitch of the coil.

The calculated inductance of the coil using the mean coil radius is $L_0 = 1.0$ microhenries. The coil inductance was measured at 17.5 megahertz using a Q meter and an RX meter. The measured L_0 values were 1.08 and 1.05 microhenries, respectively.

The inductances of the remaining portions of the circuit were obtained from measurements made using an L-C meter and a low-inductance bridge. The stray capacitance of the coil and Faraday shield was obtained by adding capacitors of known value across

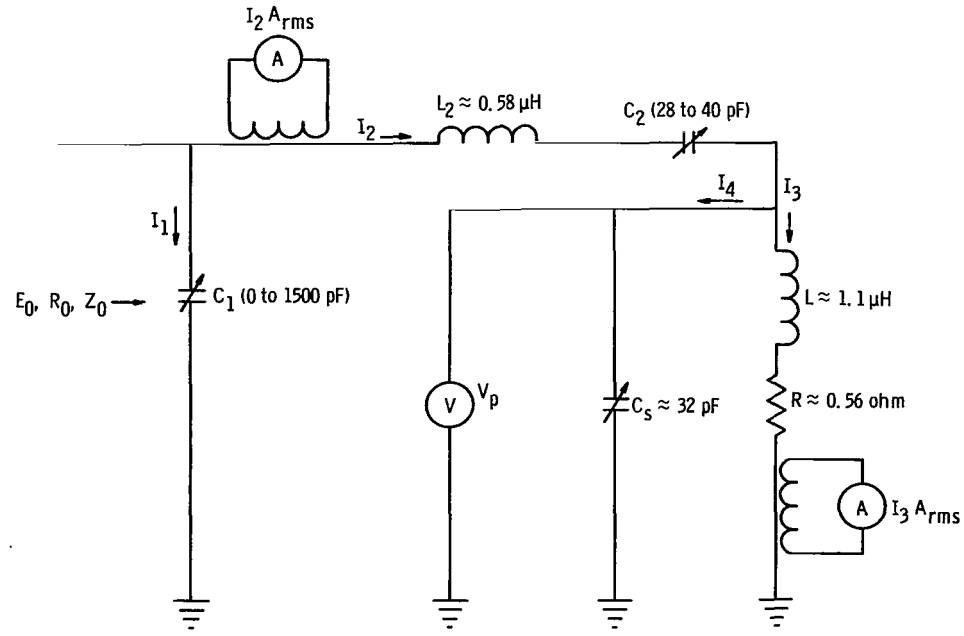

Figure 12. - Circuit parameters and measurements.

the coil and measuring the resonant frequency ω_r. If $1/\omega_r^2$ is plotted against the added capacitance, the stray capacitance may be obtained from the intercept on the abscissa axis and the inductance is the slope of the curve. The measured values of the circuit parameters as well as an indication of the measurements made during the experiments and tare data check are shown in figure 12.

When the system is tuned for zero reflected power at 17.5 megahertz the following relations hold for this circuit

$$L = \frac{6.48\ V_p(kV)}{I_3(A_{rms})} \text{ microhenries} \tag{D4}$$

$$C_s = \frac{12.74\left[I_3(A_{rms}) - I_2(A_{rms})\right]}{V_p(kV)} \text{ picofarads} \tag{D5}$$

$$Z_{eff} = \frac{V_p(kV)}{\sqrt{2}\ I_2(A_{rms})} \times 10^3 \text{ ohms} \tag{D6}$$

Where Z_{eff} is the effective impedance of the L-R-C_s portion of the circuit and was given by equation (48) as

$$Z_{eff} \approx \omega L_{ap} \tag{D7}$$

If one defines the effective inductance of the circuit as $L_{eff} = L_{ap} + L_2$ then L_{eff} is (from eq. (52))

$$L_{eff} = \frac{2.5\times10^{-3}\, C_1(pF)}{3.02\times10^{-5}\, C_1^2(pF) + 1} + \frac{82.78}{C_2(pF)} \text{ microhenries} \tag{D8}$$

The system is checked by taking a series of measurements with no plasma present. These tare results are presented in table IV. It can be seen from this table that the

TABLE IV. - CIRCUIT CHECK DATA WHEN NO PLASMA IS PRESENT

Root mean square current, I_2, A_{rms}	Root mean square coil current, I_3, A_{rms}	Peak voltage, V_p, V	Inductance, L, μH	Stray capacitance, C_s, pF	Calibrated variable capacitor		Effective inductance, L_{eff}, μH	Effective impedance, Z_{eff}, ohms	Apparent inductance, L_{ap}, μH	Inductance of strap plus lead inductance of coil, L_2, μH
					C_1, pF	C_2, pF				
			(a)	(b)			(c)	(d)	(e)	
7	12.5	2165	1.122	32.33	762	32.6	2.64	221.8	2.02	0.62
8	14.5	2510	1.121	32.96	↓	↓	↓	224	2.04	.60
9	16.3	2810	1.117	33.07	↓	↓	↓	223	2.03	.61
10	18.3	3190	1.129	33.10	↓	↓	↓	228	2.07	.57
11	20	3495	1.132	32.70	↓	↓	↓	227	2.07	.57
12	22	3815	1.123	33.30	↓	↓	↓	227	2.07	.57
13	23.8	4110	1.119	33.40	↓	↓	↓	226	2.06	.58
14	25.5	4405	1.19	33.20	↓	↓	↓	225	2.05	.59
15	27.5	4760	1.121	33.40	↓	↓	↓	227	2.06	.58
Average			1.122	33.05				225	2.05	0.588
Measured value			~1.1	~32						0.58

[a]See eq. (D4).
[b]See eq. (D5).
[c]See eq. (D8).
[d]See eq. (D6).
[e]See eq. (D7).

values of the circuit parameters obtained from the tare data agree quite well with the measured values. Therefore, we believe that the measured coil current and inductance are accurate.

In order to obtain the data when the plasma is present, the current I_3 is set and the power coupled to the plasma is obtained. The measurement of the change of inductance with a plasma is difficult because of the small magnitude of this change. It was for this reason that the change in coil inductance was determined using two methods. The first method (eq. (47) in text) used the V_p and I_3 measurements. The one shortcoming

of this method is that the L value calculated from the tare data varied slightly from day to day for various coil currents. In an attempt to overcome this problem, series of data were taken at constant coil current. The measured values of the series and shunt capacitors did remain constant for the daily tare data check when the system was tuned for zero reflected power. The second method used to calculate the inductance change was to calculate L_{ap} from these capacitor measurements (see eq. (52) in text) and obtain ΔL from equation (50).

APPENDIX E

DETERMINATION OF PLASMA RESISTIVITY

The plasma resistivity is obtained by assuming that the resistivities due to electron-atom and electron-ion collisions are additive; that is,

$$\eta = \eta_{ei} + \eta_{ea} \tag{E1}$$

When all ions are assumed to be singly charged, Spitzer (ref. 6) gives an equation for η_{ei} which becomes in SI units

$$\eta_{ei} = 65.3 \frac{\ln \Lambda}{T_e^{3/2}} \text{ ohm-meter} \tag{E2}$$

where $\Lambda = 12\pi(\epsilon_0 kT_e)^{3/2}/q^3 n_e^{1/2}$ and is tabulated in reference 6.

The resistivity due to electron-atom collisions is obtained from the equation

$$\eta_{ea} = \frac{m_e \nu'_{ea}}{q^2 f_i} \tag{E3}$$

where ν'_{ea} is the normalized electron-atom momentum-transfer collision frequency and is defined as (see ref. 14 or 15)

$$\nu'_{ea} \equiv \frac{\nu_{ea}}{n_0} = \frac{1}{3}\sqrt{\frac{32q}{\pi m_e\left(\frac{kT_e}{q}\right)^5}} \int_0^\infty \sigma_{m_{el}}(\Psi)\Psi^2 \exp\left(\frac{-q\Psi}{kT_e}\right) d\Psi \tag{E4}$$

where f_i is the fraction ionized defined as n_e/n_0.

In equation (E4), the momentum-transfer cross section for electron-atom collisions was taken from Brown (ref. 16) as a function of the kinetic energy of the electrons. The resistivity η is plotted in figure 13 as a function of electron kinetic temperature with the fraction ionized as a parameter. In this plot, the $\ln \Lambda$ was calculated using $n_e = 1\times10^{17}$ per cubic meter in the η_{ei} calculation, an assumption which causes little effect since $\ln \Lambda$ varies slowly with n_e.

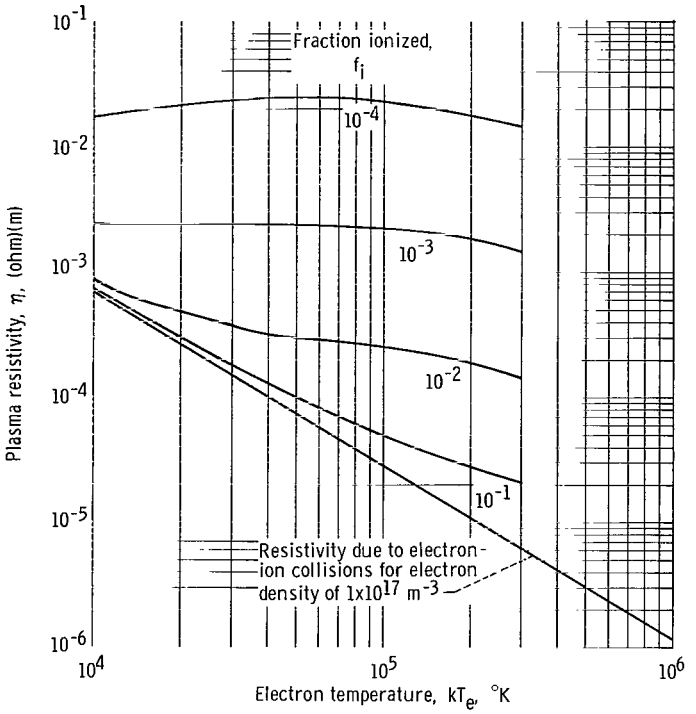

Figure 13. - Plasma resistivity as function of electron temperature with fraction ionized as parameter.

In order to determine the resistivity for the plasma under consideration, the electron density, the electron kinetic temperature, and the neutral density must be known. The electron density was obtained from the microwave interferometer data.

The electron kinetic temperature was obtained from the relative intensities of helium singlet and triplet spectral lines using the technique presented in reference 12 for tenuous helium plasmas. The 5047 and 4713 Å (504.7 and 471.3 nm) spectral lines were used, and the excitation coefficients for these lines were taken from reference 17. These spectral lines will give accurate results for electron densities below 3×10^{17} per cubic meter and will exhibit a minimum error for $3 \times 10^{17} < n_e \leq 10^{19}$ per cubic meter (see Podgornyi, ref. 18). A correction was made for cascading effects, and a study of the light emitted from a number of spectral lines indicated that the plasma did indeed fall into the tenuous regime (ref. 19). The relative wave length response of the entire system was calibrated using a standard ribbon filament tungsten lamp.

The neutral density was obtained from the McLeod gage measurements. Since the pressures in the McLeod gage and the apparatus are not necessarily equal under the near free molecular flow conditions which were present, the expression used by Chubb and Seikel (ref. 14)

$$n_0 = \frac{P_0'}{k\sqrt{T_0' T_0}} \tag{E5}$$

was used to calculate n_0 from the measured pressure. In equation (E5), P_0' is the McLeod gage pressure (N/m^2), T_0' and T_0 are neutral temperatures in the McLeod gage and discharge. Neutral temperature T_0', which should be nearly room temperature, was chosen to be 300° K. The neutral temperature of the discharge was assumed to be 450° K.

REFERENCES

1. Hittorf, W.: Ann. Physik, vol. 21, 1884, p. 137; as referenced in Hans U. Eckert, Diffusion Theory of the Electrodeless Ring Discharge, Res. Rep. 9, Convair Scientific Res. Lab., Feb. 13, 1961, ref. 1.
2. Mavrodineanu, R.; and Hughes, R. C.: Excitation in Radio-Frequency Discharges. Spectrochim. Acta, vol. 19, no. 8, 1963, pp. 1309-1317.
3. Eckert, Hans U.: A Cool Mercury Plasma Tunnel. J. Aero/Space Sci., vol. 26, no. 8, Aug. 1959, pp. 515-517.
4. Jones, Robert E.; and Palmer, Raymond W.: Experimental Investigation of a Constant-Velocity Traveling Magnetic Wave Plasma Engine. NASA TN D-2676, 1965.
5. Eckert, Hans U.: Diffusion Theory of the Electrodeless Ring Discharge. Res. Rep. 9, Convair Scientific Res. Lab., Feb. 13, 1961.
6. Spitzer, L.: Physics of Fully Ionized Gases. Second ed., Interscience Pub., 1962.
7. Abraham, Max; and Becker, Richard: The Classical Theory of Electricity and Magnetism. Second ed., Hafner Publishing Co., New York, 1949.
8. McLachlan, Norman W.: Bessel Functions for Engineers. Second ed., Clarendon Press, Oxford, 1955.
9. Hollister, Donald D.: A Technique for the Experimental Determination of the Electrical Conductivity of Plasmas. AIAA J., vol. 2, no. 9, Sept. 1964, pp. 1568-1571.
10. Swett, Clyde C.: Experiments on Inductive and Capacitive Radiofrequency Heating of a Hydrogen Plasma in a Magnetic Field. NASA TN D-2717, 1965.
11. Kuhns, Perry: Microwave Interferometer Measurements of Electron-Ion Recombination in Nitrogen, Air, and Argon. NASA TN D-1191, 1962.
12. Sovie, Ronald J.: Spectroscopic Determination of Electron Temperature and Percentage Ionization in a Helium Plasma. Phys. Fluids, vol. 7, no. 4, Apr. 1964, pp. 613-614.
13. Welsby, V. G.: The Theory and Design of Inductance Coils. Second ed., John Wiley and Sons, Inc., 1960.
14. Chubb, Donald L.; and Seikel, George R.: Basic Studies of a Low Density Half Current Ion Accelerator. NASA TN D-3250, 1966.

15. Present, Richard D.: Kinetic Theory of Gases. McGraw-Hill Book Co., Inc., 1958, p. 148.

16. Brown, Sanborn C.: Basic Data of Plasma Physics. Technology Press, M.I.T., 1959.

17. Sovie, Ronald J.; and Klein, Barry M.: Volume Ion Production in a Tenuous Helium Plasma. NASA TN D-2324, 1964.

18. Podgornyi, I. M.; and Sholin, G. V.: Note on Measurement of Electron Temperature by Helium Line Intensity Ratios. Soviet Phys. - Doklady, vol. 10, no. 1, July 1965, pp. 48-50.

19. Wilson, R.: The Spectroscopy of Non-Thermal Plasmas. J. Quant. Spectrosc. Radiative Transfer, vol. 2, Oct.-Dec. 1962, pp. 477-490.

NASA-Langley, 1967 — 25 E-3832

"The aeronautical and space activities of the United States shall be conducted so as to contribute . . . to the expansion of human knowledge of phenomena in the atmosphere and space. The Administration shall provide for the widest practicable and appropriate dissemination of information concerning its activities and the results thereof."

—NATIONAL AERONAUTICS AND SPACE ACT OF 1958

NASA SCIENTIFIC AND TECHNICAL PUBLICATIONS

TECHNICAL REPORTS: Scientific and technical information considered important, complete, and a lasting contribution to existing knowledge.

TECHNICAL NOTES: Information less broad in scope but nevertheless of importance as a contribution to existing knowledge.

TECHNICAL MEMORANDUMS: Information receiving limited distribution because of preliminary data, security classification, or other reasons.

CONTRACTOR REPORTS: Scientific and technical information generated under a NASA contract or grant and considered an important contribution to existing knowledge.

TECHNICAL TRANSLATIONS: Information published in a foreign language considered to merit NASA distribution in English.

SPECIAL PUBLICATIONS: Information derived from or of value to NASA activities. Publications include conference proceedings, monographs, data compilations, handbooks, sourcebooks, and special bibliographies.

TECHNOLOGY UTILIZATION PUBLICATIONS: Information on technology used by NASA that may be of particular interest in commercial and other non-aerospace applications. Publications include Tech Briefs, Technology Utilization Reports and Notes, and Technology Surveys.

Details on the availability of these publications may be obtained from:

SCIENTIFIC AND TECHNICAL INFORMATION DIVISION

NATIONAL AERONAUTICS AND SPACE ADMINISTRATION

Washington, D.C. 20546